Revised Manuscript highlighted

WILEY-VCH

Custom design of protein particles as multifunctional biomaterials

*Bhuvana K. Shanbhag, Chang Liu, Pradeep G.C., Tayyaba Younas, Kevin K.Y. Hu, Alex J. Fulcher, Weston B. Struwe, David Steer, Geoff Dumsday, Ian S. Harper, Philipp Kukura, Victoria S. Haritos, Lizhong He**

Dr. B.K. Shanbhag, C. Liu, Dr. P.G.C., Dr. T. Younas, K.K.Y. Hu, A.Prof. V.S. Haritos, Dr. L. He
Department of Chemical Engineering
Monash University
Clayton, VIC 3800
Australia
E-mail: lizhong.he@monash.edu

Dr. A.J. Fulcher, A.Prof. I.S. Harper
Monash Micro Imaging
Monash University
Clayton, VIC 3800
Australia

Dr. W.B. Struwe, Prof. P. Kukura
Physical and Theoretical Chemistry Laboratory
Department of Chemistry
University of Oxford
South Parks Road
Oxford OX1 3QZ, UK.

Dr. D. Steer
Monash Biomedical Proteomics Facility
Monash University
Clayton, VIC 3800
Australia

Dr. G. Dumsday
CSIRO Manufacturing
Ian Wark Laboratory
Bayview Avenue
Clayton, VIC 3168
Australia

B.K. Shanbhag and C. Liu contributed equally to the work.

Keywords: Protein particles, protein self-assembly, stimuli-responsive peptides, multi-functions, biocatalysis, biosensing

Assembled protein particles, as emerging biomaterials, have broad applications ranging from vaccines and drug delivery to biocatalysis and particle tracking, but to date these require trial-and-error rational design experimentation and/or intensive computational methods to generate. Here, we describe an easy-to-implement engineering strategy to generate customized protein proteins as multifunctional biomaterials. We utilize protein-peptide modules to generate functional nanoparticles whose assembly and size is controlled by addition of mild stimuli. The protein assembling method is versatile as exemplified through particle formation with 7 distinct protein modules, using a variety of assembly conditions tailored by the chemistries of 3 peptide partners. We have generated customized protein particles using enzymes, binding and reporter proteins, and their functions and utilities are demonstrated using biocatalysis, sensing and labelling applications, respectively. Furthermore, co-assembly with two functional proteins within one particle has been successfully achieved and demonstrated. Physical insights into the kinetics and molecular mechanisms of particle formation are revealed by small angel X-ray scattering and mass photometry, providing fundamental knowledge to guide design and manufacture these interesting biomaterials in future. Our protein assembling strategy is a reliable method for fabricating protein particle to deliver new functionalities on-demand.

1. Introduction

Protein particles have been increasingly used as biomaterials with attractive functionalities.[1,2] Particularly, those generated through the assembly of proteins into higher order structures, such as those containing multiple functionalities, is essential to their advanced applications ranging from vaccine development[3] and drug delivery[4] to biocatalysis[5,6] and biosensing.[7,8] Furthermore, directing specific structural organization of proteins is key to achieving desired functionalities such as optimal efficiency of enzymes arrays for cascade reactions,[9,10] a strong immune response elicited via high density antigen presentation through protein nanoparticles[11] and enhanced immunogenicity through multivalent displays.[12]

To date, the assembling functional proteins-based biomaterials often relies on a scaffold such as viral capsid proteins [13,14] or ferritin [11,15] although these routes have defined and limited conditions for assembly initiation. Alternative approaches utilize the fusion of target protein with designed coiled-coil peptides [16,17] or short charged tags [18] and their assembly involves the mixing of precise ratios of assembling components and/or of additional peptide components [19,20] to achieve higher order structures. Some assembling peptide partners have been modified to incorporate altered stimuli-responsive characteristics such charge [21] and light [22] to improve self-assembly of fusion proteins. For proteins, where 3-dimensional structure information is readily available, monomeric assembly units have been designed using *de novo* computational methods with capability for precise control over size, shape [23,24] and valency of assembled structure. [25,26]

Here we introduce a versatile scaffold-free protein assembling approach for the rapid preparation of functional protein particles via an integrated protein-peptide module that controls assembly. Our self-assembling approach is flexible and can be applied to various types of functional proteins including enzymes, binding and reporter proteins, and the

formation of solo, mixed or co-assembled protein particles, using a range of moderate assembly conditions to generate protein particles. The customized protein assembling strategy uses stimuli-responsive peptides to confer assembling features to proteins, without the pre-requisite for detailed structural information of proteins, to form functional particles.

In this study, we have developed a method to engineer a protein of interest that can respond to specific stimuli and assemble into particle through three simple stages (**Scheme 1**). A set of diverse protein candidates were selected with biocatalytic, binding and fluorescence capabilities including diverse structural conformation and sourced from multiple species (Figure S1). Five enzymes from four classes were tested including Tyrosinase (Class 1: Oxidoreductase), ω-Aminotransferase (Class: 2 Transferase), Cutinase (Class: 3 Hydrolases) and Carbonic anhydrases (Class 4: Lyases) from two sources (bovine (BCA) and thermophilic bacteria (TmCA)). The enhanced green fluorescent protein (eGFP) was the fluorescent protein candidate and glutathione S-transferase (GST), used popularly as an affinity tag, was chosen as the binding protein (Table S1).

First, a self-assembly peptide is selected with an assembly chemistry suited to the protein of interest. Important factors for selection of a compatible stimuli-responsive peptide partner include the characteristics of the protein of interest (physical parameters such as pI or hydrophobicity) and solution conditions of assembly that are essential for proper function of the protein. For validation, we present three characterized stimuli-responsive peptides, $P_{11}4$, Q11 and Pep-H (latter one designed in this study) with complementary chemistries influencing their stimuli sensitivity (Table S2). Previously, we have demonstrated the feasibility of formation of enzyme nanoparticles [27] using the well-known stimuli-responsive peptide $P_{11}4$[28] that is reactive to a wide set of solution conditions such as pH change, metal-ion concentration and changes in solution ionic strength.[29] The Q11 peptide [19] primarily

responds to pH and is unresponsive to magnesium ions and hence termed “metal-ion resistant peptide”. Pep-H is a peptide purposely designed in this work, to enhance hydrophobic interactions by including tryptophan and phenylalanine residues and as a result illustrates a stronger (~3-fold) hydrophobicity than $P_{11}4$ and Q11 (Table S2).

In the second stage, the protein-peptide combination is designed as a single protein construct containing the protein of interest, a chosen peptide and a flexible GS-linker between the two that provides rotational flexibility for intermolecular interactions during self-assembly. Specifically, the protein-peptide constructs were designed with the stimuli-responsive peptides fused to the C-terminus of the protein of interest via a flexible GS linker with a predicted length [30] of ~ 23 – 26 Å to allow free rotational movement of the peptide to promote intermolecular interactions during the self-assembly. The corresponding DNA sequence is inserted into a plasmid of choice, and the protein-peptide construct is expressed using a suitable host cell system. In the last stage, the purified protein-peptide is assembled into protein particles via stimuli such as change in temperature, pH or addition of ions. The protein-peptide can be assembled via one of three complementary routes: a single component particle, mixing two or more protein-peptide modules followed by assembly to form multicomponent particles, or independently mixing assembled single component protein particles into a cocktail of different particles. Additionally, the extent of stimuli can be tuned to control the formation of protein particles with a desirable size, ranging from 20-1000 nm.

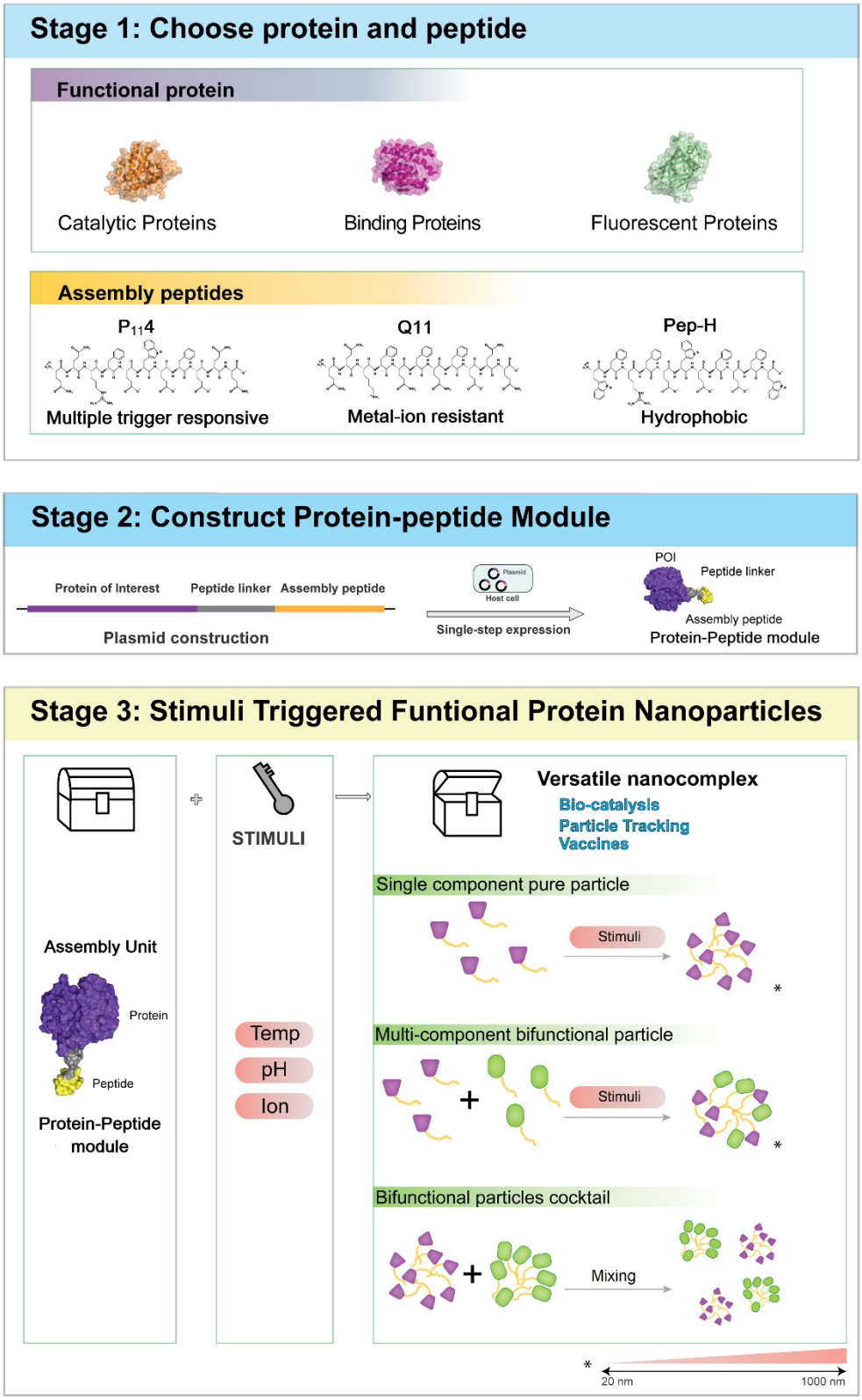

Scheme 1. Representation of the 3-stage process to produce functional protein particles involving: **stage 1**-selection of peptide partner for protein of interest, **stage 2**-construction of protein-peptide module, and **stage 3**-stimuli triggered protein particle formation and three routes for custom assembly of protein particles. *Particle size controlled by strength of stimuli (red bar)

2. Results and Discussion

2.1. A generic platform for assembling functional protein particles

We demonstrate the generic nature of our protein assembling approach by forming protein particles using seven different proteins with fluorescent, catalytic or binding functionalities as examples (**Figure 1**). Protein candidates have diverse characteristics including global symmetry, presence of disulphide bonds or metal-ion/co-factor dependencies that are important for their individual functions (biocatalysis, binder and fluorescence, Figure S1 and Table S2). Using the multi-responsive $P_{11}4$ peptide (Figure 1A), protein-peptide modules were constructed with candidate proteins, expressed and purified. A reduction of pH generated Aminotransaminase-$P_{11}4$ (ATA- $P_{11}4$), into particles (Figure 1B), whereas the addition of magnesium ions triggered the modules of tyrosinase-$P_{11}4$ (Tyr-$P_{11}4$, Figure 1C) and green fluorescent protein (eGFP- $P_{11}4$, Figure 1D) into particles.

A combination of pH change and increased solution ionic strength (via addition of 50 mM sodium nitrate) resulted in formation of Cutinase-$P_{11}4$ (Cut- $P_{11}4$) particles (Figure 1E), and for the thermostable carbonic anhydrase module (TmCA-$P_{11}4$) increased temperature generated TmCA-$P_{11}4$ particles (Figure 1F) possibly through intermolecular interactions among the TmCA-$P_{11}4$ favored by the structural fold transitions that occur over 50° C for this thermostable enzyme.[31] All protein-peptide modules had self-assembly attributes that were not observed in the corresponding unmodified wild-type proteins under the same self-assembly conditions (Figure S2). Therefore, protein-peptide modules enabled proteins to assemble as particles in response to specific stimuli.

These initial experiments demonstrated formation of single component particles and that two or more single component particle solutions may be combined to obtain a cocktail of different

proteins. The cocktail provides a simple mode to readily combine multiple functionalities in one-pot as long as the solution conditions are compatible with protein function and stability of the individual particle components. For example, two or more catalytic protein particles required for a cascade reaction must be functional under similar solution conditions.

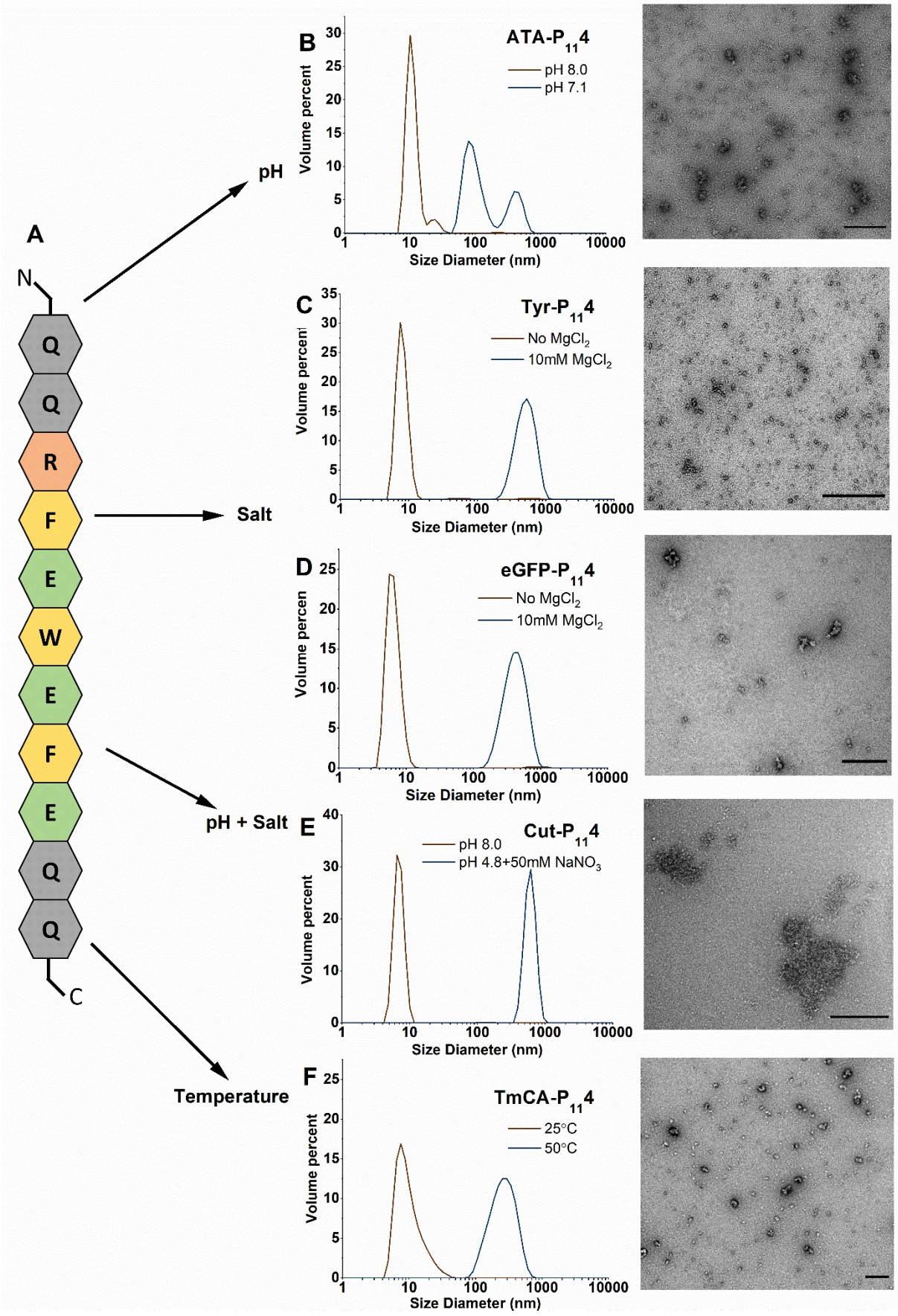
A
N
Q
Q
R
F
E
W
E
F
E
Q
Q
C
pH
Salt
pH + Salt
Temperature
B
ATA-P11A4
pH 8.0
pH 7.1
Volume percent
Size Diameter (nm)
C
Tyr-P11A4
No MgCl2
10mM MgCl2
D
eGFP-P11A4
E
Cut-P11A4
pH 4.8+50mM NaNO3
F
TmCA-P11A4
25°C
50°C

Figure 1. Assembly of a variety of functional proteins into a particle format: A) Multi-stimuli responsive $P_{11}4$ peptide and various stimuli conditions. B-F) Particle formation of various protein-peptide modules demonstrated by particle size distribution of unassembled module (brown) with assembled particles under specific stimuli conditions (blue) based on dynamic light scattering analysis (left panel) and corresponding TEM images (right panel) of protein particles formed. Scale bars, 500nm. B,) ATA-$P_{11}4$, C) Tyr-$P_{11}4$, D) eGFP-$P_{11}4$, E) Cut-$P_{11}4$, and F) TmCA-$P_{11}4$.

2.2. Expanding the scope of protein particle formation through peptide chemistry

Next, we expand the scope of protein particle formation by deploying other stimuli-responsive peptides with different chemistries. To understand how the assembly conditions are influenced by the peptide partner and protein, we prepared protein-peptide modules of three functional proteins bovine carbonic anhydrase (BCA), enhanced green fluorescent protein (eGFP) and glutathione S transferase (GST) with three peptides Pep-H, Q11 and $P_{11}4$ for a direct comparison of assembly conditions (**Figure 2**). Pep-H peptide (Figure 2A) is ~3-fold more hydrophobic than $P_{11}4$ and Q11 (Table S1), and BCA and eGFP modules designed with Pep-H showed the formation of a higher oligomeric state (ca. 10nm) even in the absence of stimuli (Figure 2B).

Since both BCA and eGFP are monomeric proteins (typical size ~5 nm), the increased size is attributed to protein assembly via the strong hydrophobic forces between peptides of individual protein-peptide modules. Because Pep-H retains glutamic acids positioned for metal-ion chelation similar to $P_{11}4$ peptide, BCA-Pep-H and eGFP-Pep-H oligomers can be assembled into larger particles by the addition of either magnesium ions (Figure 2C) or change in pH (Figure 2D) as stimuli.

Conversely, when metal ion-resistant Q11 was used as the peptide partner, neither BCA-Q11 or GST-Q11 assembled into particles after the addition of 10 mM $MgCl_2$ (Figure 2E) while

they responded well with the decrease of pH to form protein particles (Figure 2F). In contrast, the same proteins designed with the $P_{11}4$ peptide formed particles after the addition of magnesium ions (Figure 2G) or change of pH (Figure 2H). This contrasting characteristic between Q11 and $P_{11}4$ is attributed to the lack of glutamic acid residues in the Q11 peptide that are essential for metal-ion interaction.[29] Another subtle difference was observed when applying pH stimuli, where BCA-Q11 and GST-Q11 formed particles at near neutral pH (Figure 2G) but BCA-$P_{11}4$ and GST-$P_{11}4$ required a slightly lower pH (pH 6.8 and 6.0) for particle formation (Figure 2H). This feature of Q11 is beneficial for applications where the assembly of protein particles at neutral pH is required without the addition of metal ions.

By combining the findings from the application of different peptides, we demonstrated that our protein assembling method is readily adaptable to diverse stimuli-responsive peptides and the assembly condition of the constructed protein-peptide is primarily governed by peptide chemistry, and the technique can be applied to various types of proteins. Furthermore, analysis by mass spectrometry of chemically crosslinked particles confirm glutamic acid residue E265 in Pep-H and lysine residues (K15, K91, K138) from eGFP are involved in intermolecular linkages in the presence of magnesium ions (Figure 2I and 2J), confirming that interactions between the protein of interest and the self-assembly peptide plays an important role in stabilizing eGFP-Pep-H protein particles.

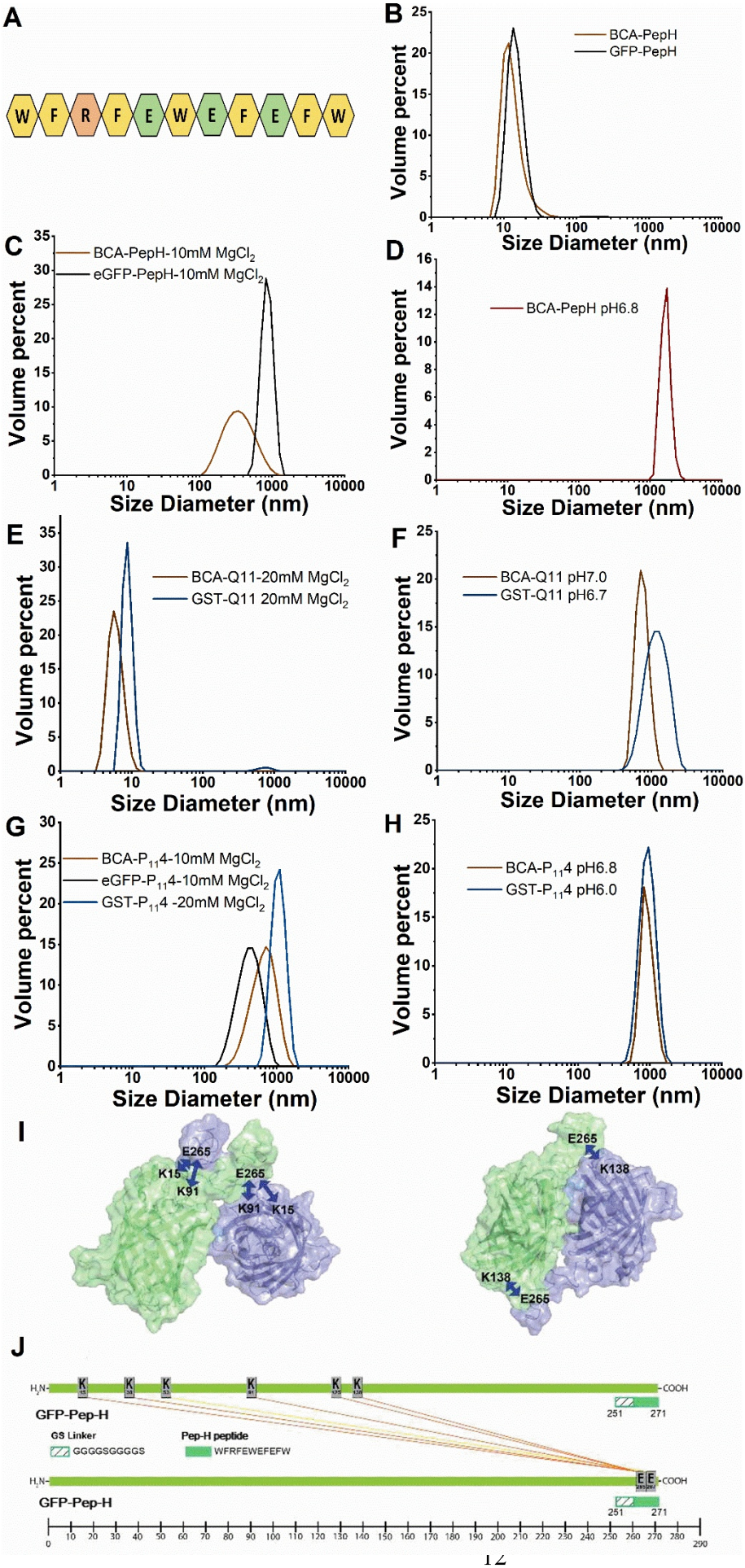
A
W F R F E W E F E F W
B
BCA-PepH
GFP-PepH
Volume percent
Size Diameter (nm)
C
BCA-PepH-10mM MgCl2
eGFP-PepH-10mM MgCl2
D
BCA-PepH pH6.8
E
BCA-Q11-20mM MgCl2
GST-Q11 20mM MgCl2
F
BCA-Q11 pH7.0
GST-Q11 pH6.7
G
BCA-P114-10mM MgCl2
eGFP-P114-10mM MgCl2
GST-P114 -20mM MgCl2
H
BCA-P114 pH6.8
GST-P114 pH6.0
I
E265
K15
K91
K138
J
GFP-Pep-H
GS Linker
GGGGSGGGGS
Pep-H peptide
WFRFEWEFEFW
COOH

Figure 2. Influence of peptide chemistry on particle assembly. A) Amino acid sequence of the designed Pep-H peptide. B-D) Particle size distribution measured by dynamic light scattering for protein-petpide modules using the Pep-H hydrophobic peptide using different stimuli: B) in the absence of stimuli, C) with magnesium, D) with pH. E-F) Particle size distribution of protein-peptide modules designed with Q11 metal-ion resistant peptide using different stimuli: E) with magnesium and F) with pH. G-H) Particle size distribution of protein-peptide modules based on the $P_{11}4$ peptide using different stimuli: G) with magnesium, and H) with pH. I) Molecular docking models of eGFP-Pep-H particles formed with magnesium. J) Intermolecular protein-peptide interaction within eGFP-Pep-H determined by cross-linking mass spectrometry.

2.3. Multi-component protein particles through co-assembly

Next, we demonstrate that the same protein-peptide modules can be successfully customized to form multi-component proteins within the same particle by co-assembling two or more proteins that are fused with the same stimuli-sensitive peptide (**Figure 3**). We selected two distinct molecules, BCA-$P_{11}4$ and eGFP-$P_{11}4$ and mixed them in their unassembled forms. The addition of magnesium ions triggers the formation of the BCA-$P_{11}4$:eGFP-$P_{11}4$ multicomponent particle. Using super-resolution STED (stimulated emission depletion) microscopy, we demonstrate that the co-assembled BCA-eGFP-$P_{11}4$ particle has both protein components within the same particle. Specific fluorophores of different excitation energies show the red STED 580nm signal (eGFP, labelled with Abberior 580) and the far-red STED 635nm signal (BCA, labelled with Abberior 635) are observed within the same protein particle (Figure 3A-C). An overlay of the two signals confirms the co-location of BCA and eGFP proteins within the same particle and this observation was consistent among particles of different sizes.

Through fluorescence spectroscopy, we illustrate a proportional change in fluorescence when different concentrations of eGFP-$P_{11}4$ (0, 5, 10, 25, 50 and 100%) were added to BCA-$P_{11}4$ and co-assembled into particles (Figure 3D). Chemical crosslinking mass spectroscopy data confirms the proximity between a glutamic acid in the $P_{11}4$ peptide (E265-eGFP) and a lysine

residue (K172-BCA) on the protein surface and is further stabilized by other protein-protein interactions [K261(BCA)-D88(eGFP); K170(BCA)-D246(eGFP); K252(BCA)-D202(eGFP)] between protein surfaces (Figure 3E). Subsequent molecular docking models of co-assembled BCA-P_{11}4: eGFP-P_{11}4 particles suggests these regions are adjacent to each other in the assembled particle structure (Figure 3F-H) and follow the same intermolecular contact principles as the single component BCA-P_{11}4 established in previous works.[29] Therefore, mixtures of protein-peptide modules possessing different functional proteins can be co-assembled into multicomponent protein particles.

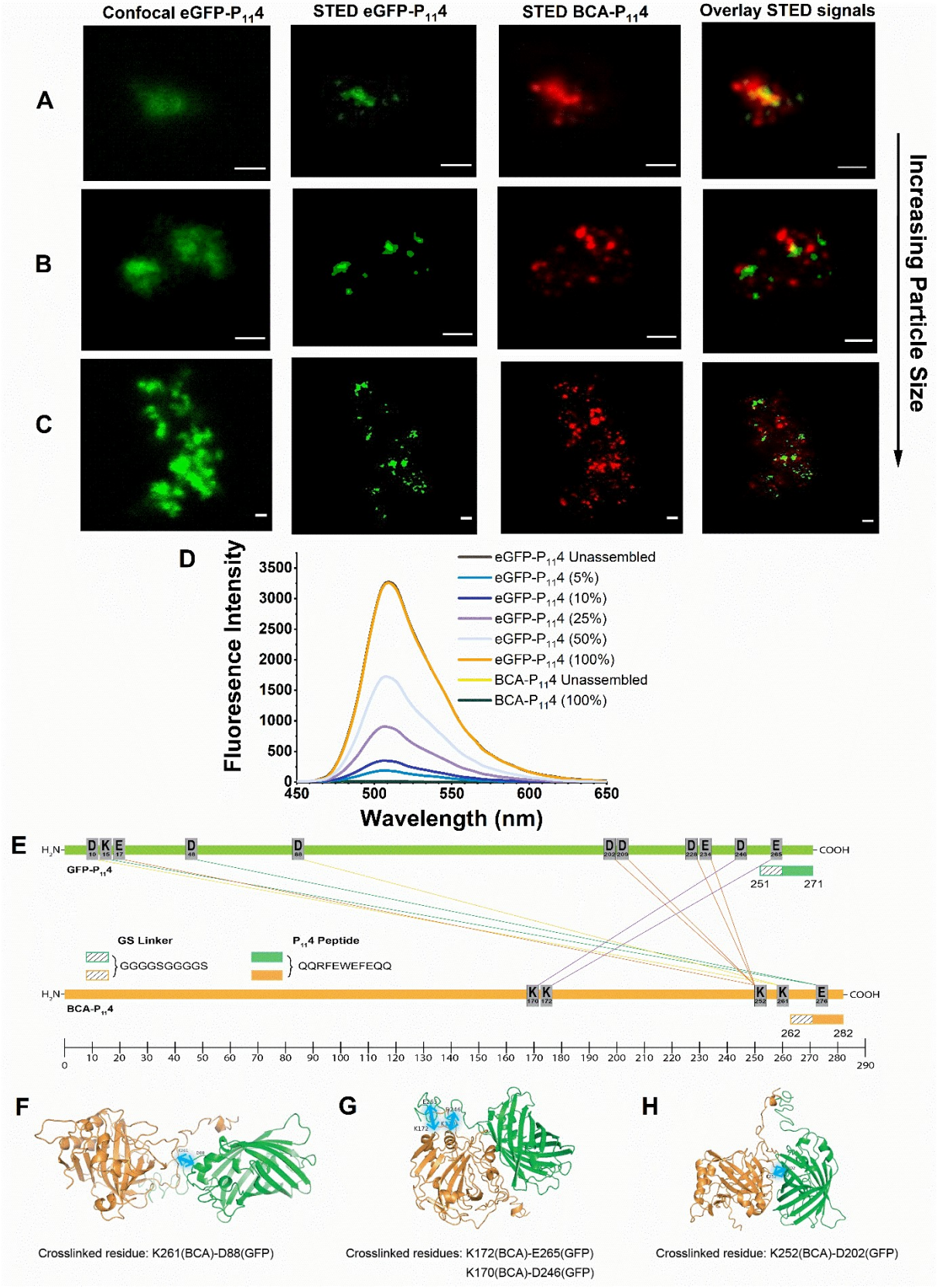

Figure 3. Co-assembly of multiple proteins to form multicomponent protein particles. A-C) Co-assembly of BCA-$P_{11}4$ and eGFP-$P_{11}4$ using magnesium ions (10mM $MgCl_2$) as stimuli. Rows - protein particles of different sizes (A-small; B-medium; C-large), Columns - different imaging signals: column 1- confocal images of eGFP-$P_{11}4$ fluorescence (green), column 2- STED images of eGFP-$P_{11}4$ (labelled with Abberior STAR 580-green), column 3- STED

images of BCA-$P_{11}4$ (labelled with Abberior STAR 635-red), column 4-overlay of STED signals of eGFP-$P_{11}4$ and BCA-$P_{11}4$). Scale bars, 500nm. D) Relative change in fluorescent intensity of BCA-$P_{11}4$:eGFP-$P_{11}4$ particles based on different ratios (0, 5, 10, 25, 50 and 100%) of eGFP-$P_{11}4$ mixed with BCA-$P_{11}4$ to form the co-assembled particles. E) Protein-protein interactions within the co-assembled particle using crosslinking mass spectra data. F-H) Molecular docking models of co-assembled BCA-$P_{11}4$:eGFP-$P_{11}4$. Blue double headed arrows are crosslinked amino acids.

2.4. Functional protein particles - a 'versatile biomaterial'

The functionalities of protein particles are illustrated by a combination of biocatalysts, gold particle labeling and flow cytometry (**Figure 4**). Protein particles that contain enzymes were functionally evaluated for catalytic activity and compared with their unassembled counterparts and unmodified enzymes. All particles tested retained >80% of the enzyme activity compared to their unassembled counterparts (Figure 4A) and retained activities similar to the wild-type enzyme (no added peptide), illustrating the protein-peptide design principles allowed for retention of protein functionality.

Earlier we have shown using STED microscopy that co-assembled protein particles are readily labelled using standard immunofluorescence. We further expanded the utility of labelling of protein particles through direct immunogold labelling against eGFP within a co-assembled BCA-Pep-H: eGFP-Pep-H particle (equal ratio). The TEM image shows the binding of two gold nanoparticles on the surface of BCA-Pep-H: eGFP-Pep-H particle (Figure 4B). This provides a new route to include a third function through selective coupling of transition metals and inorganic components to develop a new generation of hybrid bio-inorganic materials. Particularly, the coupling of inorganic components with biological particles provides the proximity required for application in asymmetric catalysis utilizing enzymes and transition metals such as gold [32] and for bioimaging using bio-inorganic hybrid quantum dots.[33]

In case of fluorescent protein particles, we demonstrate that eGFP-$P_{11}4$ particles are readily distinguishable from non-fluorescent particles (BCA-$P_{11}4$) in a cocktail of assembled particles based on the different fluorescent intensity profiles when analyzed by flow cytometry (Figure 4C). Furthermore, the eGFP-$P_{11}4$ particles were clearly differentiated from other sub-populations (intermediate structures and monomers) based on their relative size profiles (Figure 4D).

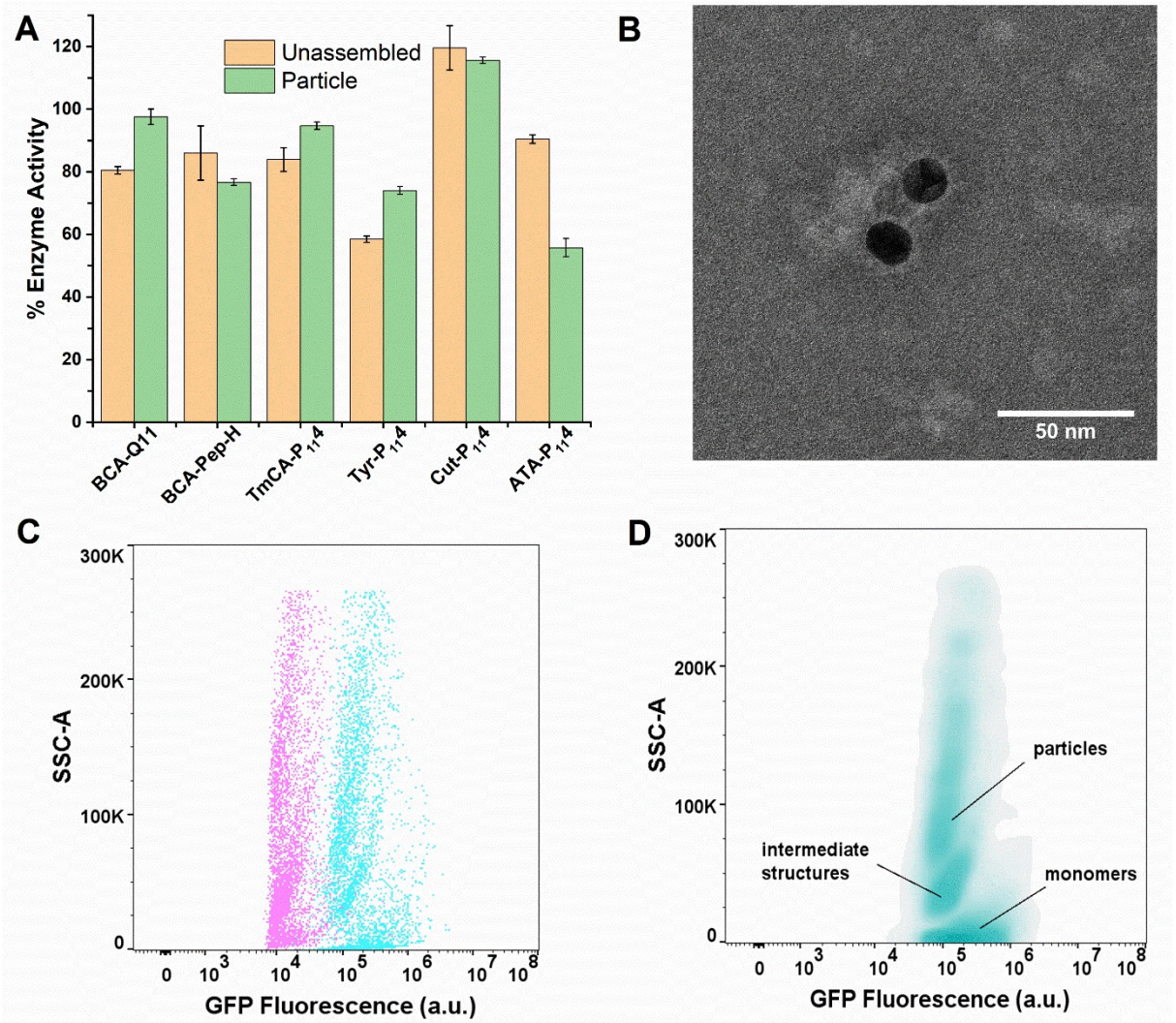

Figure 4. Functional evaluation of protein particles formed using different assembly routes. A) Biocatalytic activities of single component particles in comparison with their respective unassembled enzymes relative to their corresponding wild-type enzymes (100%). B) TEM image of co-assembled BCA-Pep-H: eGFP-Pep-H particle labelled with inorganic gold nanoparticles. C) Detection of fluorescent particles using flow cytometry-eGFP-P_{11}4 particles (Cyan), BCA-P_{11}4 particles (Magenta). D) Differentiation of eGFP-P_{11}4 particles sizes using flow cytometry.

2.5. Physical insights into characteristics of protein particle assembly

We obtain further physical insights of particle formation using small angle X-ray scattering (SAXS) and mass photometry (MP) (**Figure 5**). Particle formation of BCA-P_{11}4 triggered by magnesium ions was monitored by SAXS in a time-resolved fashion. In Figure 5A, SAXS intensity curves show an increasing trend at the lower q range ($q<0.05Å^{-1}$), indicating the presence of particles that are larger in size than that of the unassembled BCA-P_{11}4. This is more noticeable from the scattering profiles at $q<0.01Å^{-1}$ showing particle formation occurring within 10 secs of exposure to stimuli (Figure 5A-inset). Furthermore, extrapolated intensity values at zero angle demonstrate the steady growth of BCA-P_{11}4 up to 110 secs post addition of ions that stabilizes after ~140 secs, confirming particle formation occurs within a short timescale of < 2 mins (Figure 5B). The formation of higher oligomeric states of BCA-P_{11}4 using reduced pH as stimulus was visualized at different pH using mass photometry (MP).[34] In Figure 5C, single particle images of BCA-P_{11}4 at different pH during the assembly process are compared. At pH 8, BCA-P_{11}4 exists as monomers whereas reduction of pH to 7.2 or 6.8 initiates particle assembly. Based on differential MP images, we mapped the progression of BCA-P_{11}4 particle formation from a monomeric state (pH 8 blue region), through assembly initiation (pH 7.2- 6.8 orange region) and stable protein particles (pH <6.8 green region), where an increase in image size and contrast indicate BCA-P_{11}4 is assembled at a higher oligomeric state (Figure 5C).

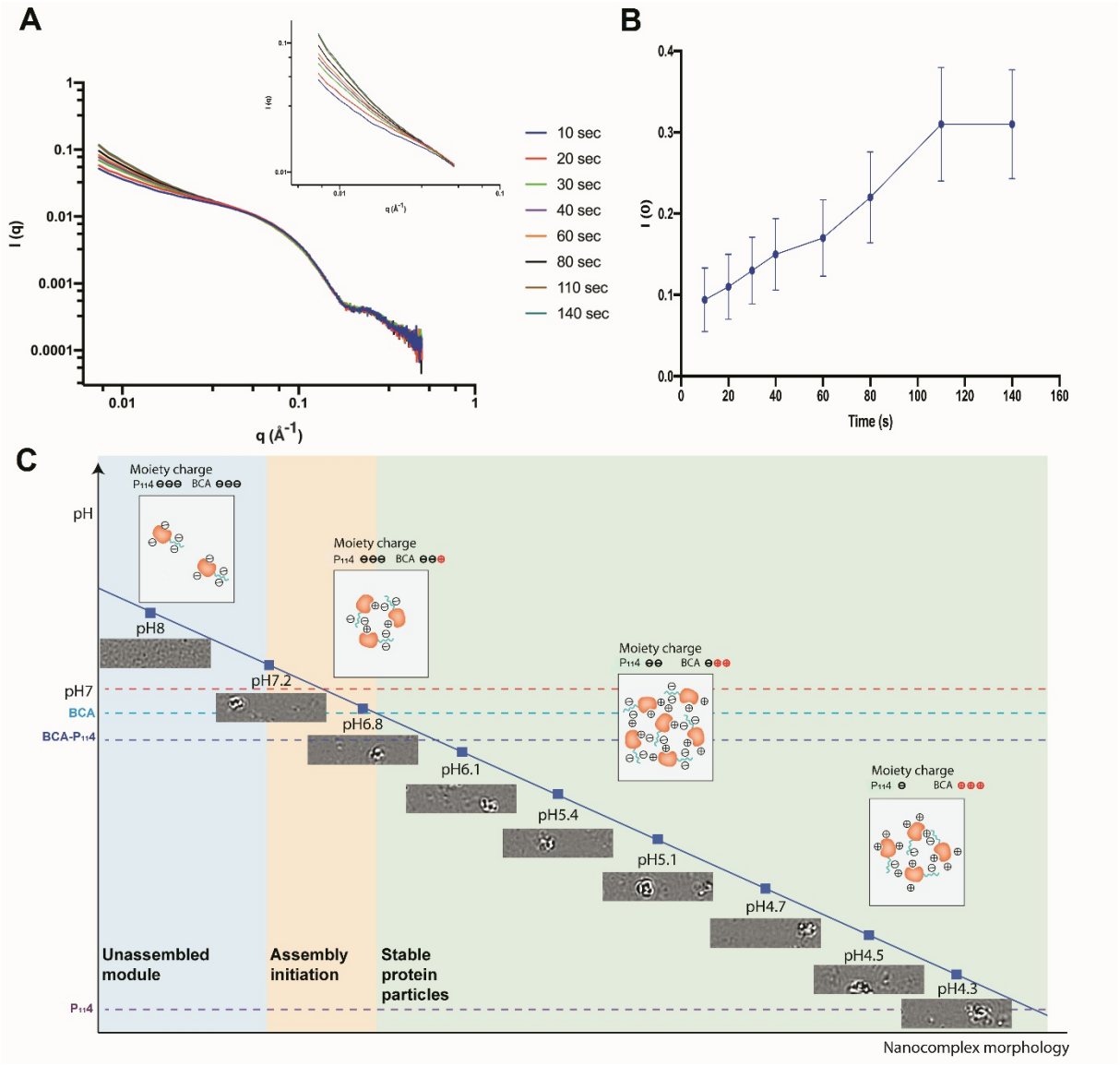

Figure 5. Physical insight of BCA-P$_{11}$4 particle formation. A) Timeframes of BCA-P$_{11}$4 particle assembly kinetics triggered with 10 mM $MgCl_2$ illustrated by small angle scattering (SAXS) curves, Inset: SAXS curves at low angle from 0 to 0.1Å^{-1}. B) Intensity values at zero angle indicating increasing particle size of BCA-P$_{11}$4 over time. C) Growth of unassembled BCA-P$_{11}$4 into stable particle with pH reduction (solid blue line) as stimulus monitored by mass photometry (MP)- Unassembled state (blue shaded region), Assembly initiation (orange shaded region) and stable protein particles (green shaded region). Dotted horizontal lines indicate the pIs of BCA (blue), BCA-P$_{11}$4 (purple) and P$_{11}$4 peptide. Inset below pH line: MP image of single particle at respective pH points (blue squares). Inset above pH line: cartoon representation of likely protein-protein interactions based on charge.

3. Conclusions

Our protein particle assembly approach described here can be readily customized and applied to generate different functional proteins with minimal modification. Stimuli-responsive

peptides such as $P_{11}4$ are known to self-assemble gradually into nanofibrils above a critical peptide concentration (10 mg mL^{-1} for $P_{11}4$).[35] Although the protein-peptide modules reported here utilizes a single stimuli-responsive peptide in its design, the formation of protein particles occurs well below the critical concentration of the peptides. The modular design uses one terminus of the protein chain to link the stimuli-responsive peptide, leaving another terminus available for further functionalization to make versatile biomaterials. The characterized peptide set demonstrated here offers a wide choice of stimuli and/or combinations of stimuli to generate protein particles, with the flexibility to suit the function and purpose of the protein of interest. Importantly, protein particles formed using this method assemble quickly as confirmed by SAXS and MP.

Another highlight is that the same protein-peptide module can be assembled into a single, cocktail or multi-protein particle without the need to redesign the building block. Such a universal building block is convenient from a material production perspective and provides great versatility for a variety of applications. Co-assembly of multiple functional proteins is key to generating a synthetic metabolon,[36] multi-enzyme reactions[37] or heterogeneous catalysis.[38,39] Using the co-assembly approach one can also generate protein particles that have multiple antigenic epitopes suitable for use as a vaccine, with greater flexibility in controlling particle size with stimuli, complementary to similar nano-vaccines using nanofiber[40] or VLP, but with a much simpler manufacturing process. Our self-assembly approach can be used to assemble a protein of choice as a coating over polymer or inorganic nanoparticles for targeted drug delivery applications in addition to the known benefits of shielding against blood proteins and reduced nanoparticle clearance by the immune system.[41] Alternatively, assembled protein particles may provide sites for drug conjugation through molecular interaction and its subsequent release.[7] Moreover, the insights revealed by controlled molecular assembly of pure drug nanoparticles[42] could be applied to protein

particle assembly for advanced drug delivery platforms. Fluorescent protein-based particles can be used in conjunction with single-particle tracking technology[43] for the direct observation of cellular processes within biological systems. For example, conjugation of fluorescent protein particles with tumor-specific aptamers may aid cancer therapy through improved detection of tumor cells.[7,44] The particle structures formed are stable under fluid flow conditions as demonstrated via flow cytometry analysis with potential application as protein-based fluorescent beads. The protein particles formed are stable to labelling procedures hence provide options for add-on orthogonal functions such as selective coupling of transition metal nanoparticles or imaging fluorophores via immuno-labelling. Protein particles offer a functional scaffold for selective coupling of inorganic constituents which in turn provide complementary properties of strength, higher refractive index and density not intrinsic to proteins,[45] thereby expanding the scope into hybrid bio-inorganic materials. The protein particles presented herein were prepared manually, however, the process can be readily automated and scaled for rapid manufacture or scaled-down using microfluidic devices for high-throughput applications.[46]

In summary, our protein particle assembling method is a versatile for production of protein particles as functional biomaterials using stimuli in a controlled manner. The rational design of the protein-peptide module is time-efficient and readily applied to a variety of functional proteins with little or no reliance on structural information. The convenience of design and three-step process to assembly makes it comprehensive yet easy-to-implement method to create protein particles under specific desired conditions for an intended application. We envisage the versatile and adaptable features of our protein particle assembling approach will open new opportunities for the generation of customized multifunctional protein particles.

4. Experimental Section

Plasmid and Bacterial expression: Two plasmids were constructed for each of the selected protein candidates, one containing the gene for the WT-protein (unmodified) and the other with gene for the corresponding protein-peptide fusion. The fusion construct for each protein was designed with one self-assembly peptide attached to the C-terminus via GGGGSGGGGS linker sequence, and a total of 11 fusion constructs with different combinations of proteins and peptides were constructed. The amino acid sequences of all protein-peptide fusion constructs designed for this study are shown in Supplementary Table S3. All gene sequences were codon optimized for *E. coli* expression, synthesized, and ligated into pET28a expression plasmid between *NcoI*- *XhoI* or *NdeI*- *XhoI* restriction sites by GenScript (Piscataway, NJ, USA). The WT-TmCA-pET28a plasmid was a kind gift from Michelle Williams (CSIRO Land and Water, Australia). All plasmids were transformed into *E.coli* BL21 (DE3) competent cells (#C2527H, NEB, Australia) except for plasmids for WT-Cutinase and Cutinase-$P_{11}4$ that were transformed into SHuffle T7 express cells (#C3029J, NEB, Australia) using supplier recommended High Efficiency Transformation protocol (NEB#C2987). Proteins were expressed by growing the *E. coli* constructs in terrific broth (TB) supplemented with kanamycin (50 µg mL^{-1}) and 0.2% v/v lactose (autoinduction) and a 2% v/v inoculum. Cultures were grown at 37°C for 4 hours with shaking at 200 rpm and then where specified, induced with IPTG (concentrations ranging from 0.1 mM to 1 mM) at 20 °C. Protein expression using SHuffle T7 express cells were performed as above except the growth temperature was reduced to 30°C. Detailed growth and expression conditions are described in Supplementary Table S4.

Protein purification: Purification for all proteins was undertaken using the following procedure. Briefly, cells were harvested by centrifugation at 8,000 × g (Sigma 6-16K, John Morris Scientific) for 10 min at 10°C. Cell pellets (2.5 to 5 g) were re-suspended in lysis buffer (50-60 mL) and incubated for 20 min at room temperature with low-speed mixing.

Each cell suspension was placed in an ice bath and lysed using sonicator (QSonica, Q125) equipped with 2 mm probe at 90% amplitude with 10 sec pulse ON and 20 sec pulse OFF for total time of 5 min. (Note: For cutinase, cell pellet was re-suspended in BugBuster® Protein Extraction Reagent lysis buffer (Merck Millipore) and incubated for 20 min at room temperature with low-speed mixing and sonication was avoided). The cell lysate was clarified by centrifugation at 16,000 × g (Sigma 6-16K, John Morris Scientific) at 10°C for 20 min. The resulting supernatant was filtered through a 1.2 µm filter followed by a 0.45 µm filter prior to purification. Purification was performed on a 5 mL HisTrap FF (GE Healthcare) immobilized metal-ion affinity chromatography charged with nickel ions using AKTA start™ Chromatography system. The column was equilibrated and washed using 5 column volumes of binding buffer. In some cases, a second washing step was used to remove contaminating proteins. Bound proteins were eluted stepwise. Each step was at least 3 column volumes. Fractions were pooled based on purity determined by SDS-PAGE 4-12% Bis-Tris Bolt gels and pooled eluate was desalted using size exclusion chromatography on a G25 Sephadex (GE Healthcare) column (1.5 × 17 cm) with a desalting buffer. Purified samples were stored at 4°C in desalting buffer before analysis. The specific buffers used for each protein are tabulated in Supplementary Table S5. Identical purification protocols were performed for WT-proteins and their corresponding fusion system.

Preparation of Protein particles: Stimuli conditions such as alteration of pH, addition of metal ions, adjusting ionic strength and change of temperature were explored to initiate the formation of protein nanoparticles for the proteins fused with self-assembly peptide. Briefly, purified protein solutions with protein concentration of 0.4-0.5 mg mL^{-1} in an appropriate buffer was used to test different stimuli. The pH stimulus was tested using purified proteins dissolved in 50 mM Tris-HCl pH 8.0 followed by a stepwise reduction of pH using 5 M or 1 M acetic acid to achieve the desired pH. Stimulus with magnesium ions was tested with purified

proteins dissolved in appropriate Tris-HCl buffer supplemented with $MgCl_2$ to a final concentration of 5 mM-20 mM for 5 min at 25 °C using a $MgCl_2$ stock solution prepared in the same Tris-HCl buffer as used for purified protein. Temperature induced self-assembly was tested by incubating protein solutions dissolved in appropriate buffers for 1 min at different temperatures (25, 30, 40 and 50 °C) within the chamber of a Zetasizer Nano ZS (Malvern Panalytical, UK). The optimal method for each protein-peptide system is summarized in Supplementary Table S6. Particle formation was monitored by Dynamic Light scattering using the Zetasizer Nano ZS (Malvern Panalytical, UK) and particle sizes determined in triplicate measurements each consisting of 10 measurement cycles. The same conditions were applied for WT-proteins as controls.

Co-assembly of multifunctional particles: Multi-functional protein particles where prepared by mixing a known ratio of two purified protein-peptide modules and triggering with appropriate stimuli. Specifically, to generate the $P_{11}4$ peptide based multi-functional protein particles, purified BCA-$P_{11}4$ and eGFP-$P_{11}4$ solutions were diluted to 0.5 mg mL^{-1} in 10 mM Tris-HCl pH 8 and eGFP-$P_{11}4$ was added to the BCA-$P_{11}4$ solution at different ratios (5, 10, 25, and 50%) with a constant final volume (1 mL). To each mixture, $MgCl_2$ was added from a 0.5 M stock solution prepared in 10 mM Tris-HCl pH 8 buffer to a final concentration of 10 or 20 mM and incubated for 5 mins at 25°C followed by particle analysis by Dynamic Light scattering.

Multifunctional Protein particle imaging using Super-resolution STED microscopy: Mixed protein particle samples with BCA-$P_{11}4$ and GFP-$P_{11}4$ were labelled with fluorescent dyes via indirect immuno labelling using suitable primary and secondary antibodies. BCA-$P_{11}4$ was labelled with primary rabbit Anti-Carbonic Anhydrase II antibody (AB7001, abcam, Melbourne Australia) and secondary goat anti-rabbit antibody conjugated with abberior

STAR 635 (ST635-1002, Abberior GmbH). eGFP-$P_{11}4$ was labelled with primary mouse Anti-GFP mABs (Antibody and Protein Therapeutics-Protein Production Unit, Monash University Australia) and secondary goat anti-mouse antibody conjugated with abberior STAR 580 (ST580-1001, Abberior GmbH). BCA-$P_{11}4$ and eGFP-$P_{11}4$ (0.5 mg mL^{-1}) were mixed in equal ratios and $MgCl_2$ was added to a final concentration of 10 mM to form co-assembled protein particles. Immunolabelling was performed by incubating the co-assembled particle solution sequentially, first with primary mouse Anti-GFP mABs for 1 hour at medium speed on a platform rocker. The sample was added to Capto core 700 beads (40 µL) (GE Healthcare) pre-washed with 10 mM Tris-HCl pH 8 and incubated on the rocker for 15 mins to remove the unbound primary antibodies. The treated sample was retrieved by collecting the supernatant following centrifugation at 3000 ×g for 5 mins. Next, primary Anti-Carbonic Anhydrase II antibody was added to the same sample and incubated for 45 mins followed by Capto core beads treatment as described above. Finally, both secondary antibodies conjugated with Abberior STAR dyes were added together to the protein particle mixture bound with primary antibodies and incubated on the rocker for 45 mins. The Capto core bead procedure was repeated and the supernatant solution containing labelled protein particles was used for coverslip preparation. Labelled protein particles (10 µL) was placed on poly-L-lysine coverslip and sealed over a glass slide using silicone-glue Twinsil® (Picodent, Wipperfürth, Germany, #13001000) and allowed to set before using for STED (stimulated emission depletion) imaging.

Super-resolution microscopy of dual function protein particles (BCA-$P_{11}4$ and eGFP-$P_{11}4$) was performed using the Abberior STED (Abberior Instruments GmbH, Gottingen, Germany) with an Olympus IX83 body, with ×100/1.4NA (UPLSApo, 0.13mm WD). Super-resolution imaging was performed using the STED 775 nm depletion laser with a 561 nm and a 640 nm excitation laser. Confocal imaging was performed under the same conditions, with the 488

nm excitation laser to obtain eGFP-$P_{11}4$ images. The Imspector software was used to collect the confocal and STED images (20nm x,y pixel) which were processed using biological-image analysis software Fiji[47].

Cross-linking of protein particles and mass spectrometry analysis: The chemical cross-linking experiments were performed as described in a previous study.[29] Briefly, eGFP-Pep-H (~32 μM) was prepared in 20 mM potassium phosphate buffer and particle formation triggered with $MgCl_2$ at a final concentration of 10 mM. To produce multiprotein particles, an equimolar (16 μM) ratio of proteins BCA-$P_{11}4$ and eGFP-$P_{11}4$ was prepared in 20 mM potassium phosphate buffer and $MgCl_2$ added at 10 mM final concentration to trigger multiprotein particle formation. After confirming particle formation using dynamic light scattering, the particle sample (40 μL) was subjected to chemical crosslinking. The crosslinking reaction was initiated by the addition of 10 mM EDC/ 5 mM sNHS (Sigma-Aldrich) and incubated at room temperature for 15 min before quenching with 1 M Tris-HCl, pH 7.

The crosslinked protein particles were separated on SDS-PAGE gel (Bolt 4−12% bis-Tris Plus Gels, Invitrogen). After the Coomassie blue staining procedure, the gel band corresponding to crosslinked protein particles with an elevated molecular weight, was excised for mass spectrometry analysis. The excised gel bands were routinely digested with trypsin and analyzed by nanoLC-ESI-MS/MS. *In silico* identification of crosslinked peptides was performed using Byonic. Molecular docking models of crosslinked proteins were generated using FRODOCK.[48]

Functional Assay 1: Enzyme Activity assays: Functional analysis of monomeric enzyme-peptide constructs and their particulate forms were analyzed using assays specific for each protein. Protein particle samples were first prepared using the optimal initiation conditions for each

protein-peptide system prior to measurement of enzyme activity. For all assays, a blank sample was prepared using assay buffer and substrate with water replacing the enzyme solution. Absorbance was measured using a microplate reader (Infinite 200 PRO, Tecan). Following blank correction of absorbance, the slope in terms of absorbance per sec was calculated as the rate of reaction.

Carbonic anhydrase activity was measured using para-nitrophenyl acetate (pNPA) as substrate.[29] The assay was performed in a 96 well assay plate using a reaction mixture (50 mM sodium sulphate + 50 mM HEPES pH 8.0 (for BCA) and 1 M sodium sulphate + 50 mM HEPES pH 8.0 (for TmCA), enzyme (3 µg) and 1 mM pNPA in a final reaction volume (0.2 mL). Absorbance was measured at 405 nm every 30 sec for 15 min.

Tyrosinase activity was measured in a 96 well plate using a reaction mixture containing 50 mM Tris-HCl + 0.01 mM $CuSO_4$ pH 7.5, enzyme (3 µg) and L-tyrosine as substrate (1mM) in final assay volume (0.2 mL). Absorbance was measured at 475 nm every 15 sec for 8 min. [49]

Cutinase activity was determined using para-nitrophenyl butyrate (pNPB) as the substrate at concentrations 0.1 and 0.5 mM. The assay was performed in a 96 well assay plate using reaction mixture containing 50 mM Tris-HCl pH 8.0 +10 mM NaCl and enzyme (0.35 µg) in final assay volume (0.2 mL). Absorbance was measured at 405 nm every 15 sec for 2 min. Aminotransaminase (ATA) activity was measured using α-methylbenzyl amine (-MBA) as the substrate using solutions of 2.5 mM (R)- or (S)-α-MBA and pyruvate mixed with the purified enzyme. An increase in absorbance at 245 nm was correlated to the formation of acetophenone.[50]

Functional Assay 2: Fluorescent Measurement Assay: Fluorescence of eGFP-peptide protein particles was measured using the TECAN infinite PRO plater reader. The protein samples were diluted to a concentration of 0.5 mg mL^{-1} prior to measurement. The excitation wavelength was 400 nm, and the emission was 450 nm with a bandwidth of 5 nm for each wavelength.

Negative Staining, Immuno-gold staining and Transmission Electron Microscopy:

The negative staining procedure was performed with protein particle samples at a concentration range of 0.2-0.5 mg mL^{-1}. Carbon coated 200 mesh copper grids (GSCu200CC, Proscitech, QLD Australia) were glow-discharged for 30 sec. Protein particle samples (5-10 µL) were applied on to the glow-discharged grids and incubated for 5 min at room temperature. Following incubation, grids were blot dried using filter paper to remove excess protein solution. The grids were washed twice with water (20 µL) of followed by a first short staining with 2% v/v uranyl acetate (25 µL drop) and then a second staining step of 30 sec. Excess stain was removed using filter paper. The grids were air dried prior to imaging. Immunogold staining was performed on multi-protein particle samples containing a mixture of BCA-Pep-H and eGFP –Pep-H in equal ratio. Briefly, BCA-Pep-H: eGFP-Pep-H particle sample (50 µL) was incubated with Anti-GFP gold antibody (1 µL) (Biorbyt Ltd. Cambridgeshire, UK) for 1 h at room temperature on a slow shaking rocker. After incubation, the labelled sample was treated with Capto core 700 beads (40 µL) (GE Healthcare) pre-washed with 10 mM Tris-HCl pH 8 and incubated for 15 mins with gentle rocking. Gold-labelled protein particles were retrieved by centrifuging the sample at 3000 x g for 5 mins. The supernatant was collected and subjected to same negative staining procedure used for TEM imaging.

Samples were viewed using a transmission electron microscope at 200 kV (FEI, Tecnai G2 T20 TWIN LaB6) and electron micrographs were recorded using CCD camera and Gatan "Digital Micrograph" software. Particle size distribution and transmission electron microscopy image analysis was performed using ImageJ software [51].

Flow Cytometry of Protein particles: Protein samples in both their monomeric and particle forms were analyzed by flow cytometry. Both eGFP-$P_{11}4$ and BCA-$P_{11}4$ particle samples were enriched by treatment with Capto core 700 beads (40 µL) (GE Healthcare) pre-washed with 10 mM Tris-HCl pH 8 and incubated for 15 mins with slow shaking. Samples was centrifuged at 3000 x g for 15 min and the supernatant was used for flow cytometry analysis. Flow cytometric readings were acquired using a 488 nm excitation laser and an FITC (525 nm/40 nm BP) emission filter (CytoFlex flow cytometer, Beckman Coulter). Acquisition threshold was set to be either solely based on the detected FITC signal (FITC) or in combination with forward scattering signal (FSC) under automatic mode. Samples were recorded at a flow rate of 10 µL min^{-1}. Flow cytometric data were analyzed and processed with CytExpert software v2.3 (Beckman Coulter) and FlowJo software v10.6.1 (FlowJo LLC).

Small angle X-ray scattering (SAXS) measurements and analysis: SAXS measurements were performed using the SAXS/WAXS beamline at the Australian Synchrotron.[52] The protein sample or buffer was loaded into a quartz glass capillary with a 1.5 mm path length using a Solution Autoloader from a 96 well plate. The scattered radiations from sample at ambient temperature were collected with a measurement interval of 1 second using Pilatus 3X 2M detector located ≈1.5 m away, giving a scattering vector q range of 0.01 – 0.51 $Å^{-1}$. Calibration of the sample to detector distance, normalization of scattering intensity to an

absolute scale, and buffer background subtraction were carried out using an established protocol.[52] The kinetics of protein particle formation was studied for a duration of 150 sec. SAXS data analysis was carried out using the data analysis package from the European Molecular Biology Laboratory (EMBL) Hamburg outstation. To obtain the radius of gyration and the pair distribution function *p(r)*, the indirect Fourier transformation (IFT) method was performed by the program GNOM using perceptual criteria.[53]

Mass photometry (MP): Data was acquired using a Refeyn OneMP (Refeyn Ltd., Oxford, UK) and an equivalent instrument built in-house as described.[34] Unassembled BCA-P_{11}4 prepared in 50 mM Tris-HCl pH 8 was diluted to 100 nM and aliquoted into multiple samples (500 µL). Particle formation was initiated by reducing the pH via addition of acetic acid to sample and immediately loading the sample onto the mass photometry coverslips (prepared with gaskets). Data was recorded for several minutes per measurement with the following instrument settings: acquisition frame rate of 955 Hz and pixel binning of 4x4 with 5-fold frame averaging. Data were analyzed with DiscoverMP (Refeyn Ltd., Oxford, UK).

Supporting Information

Supporting Information is available from the Wiley Online Library or from the author.

Acknowledgements

B.K.S and C.L. acknowledge the Monash University Institute of Graduate Research for scholarship. C.L. acknowledges the travel grant provided by Faculty of Engineering, Monash University. P.G.C acknowledges the New Horizon Research Scholarship provided by Faculty of Engineering, Monash University and Commonwealth Scientific and Industrial Research Organization (CSIRO), Australia. V.H. acknowledges the financial support from LIEF grant number LE16100185. B.K.S and L.H. acknowledges the support from the Australian Research Council (ARC) through the ARC Research Hub for Energy-efficient Separation (IH170100009). We acknowledge the facilities of Monash Micro Imaging, Monash Centre for Electron Microscopy, The Clive and Ramaciotti Centre for Structural Cryo-Electron Microscopy and Monash Biomedical Proteomics for their services. The authors thank Dr. Tim Ryan and Dr. Adrian Hawley from the Australian Synchrotron for technical support of SAXS work and Gina Pacheco Arredondo for her assistance with SAXS experiments. B.K.S and C.L contributed equally to this work.

Conflict of Interest

The authors declare no conflict of interest

Received: ((will be filled in by the editorial staff))
Revised: ((will be filled in by the editorial staff))
Published online: ((will be filled in by the editorial staff))

References

[1] W. C. Mak, R. Georgieva, R. Renneberg, H. Bäumler, *Adv. Funct. Mater.* **2010**, *20*, 4139.

[2] S. Sridharan, M. B. J. Meinders, L. M. Sagis, J. H. Bitter, C. V. Nikiforidis, *Adv. Funct. Mater.* **2021**, *2101749*.

[3] L. Deng, T. Mohan, T. Z. Chang, G. X. Gonzalez, Y. Wang, Y. M. Kwon, S. M. Kang, R. W. Compans, J. A. Champion, B. Z. Wang, *Nat. Commun.* **2018**, *9*, 359.

[4] Y. Hsia, J. B. Bale, S. Gonen, D. Shi, W. Sheffler, K. K. Fong, U. Nattermann, C. Xu, P. S. Huang, R. Ravichandran, S. Yi, T. N. Davis, T. Gonen, N. P. King, D. Baker, *Nature* **2016**, *535*, 136.

[5] R. Frey, T. Hayashi, D. Hilvert, *Chem. Commun.* **2016**, *52*, 10423.

[6] M. J. Lee, J. Mantell, L. Hodgson, D. Alibhai, J. M. Fletcher, I. R. Brown, S. Frank, W. F. Xue, P. Verkade, D. N. Woolfson, M. J. Warren, *Nat. Chem. Biol.* **2018**, *14*, 142.

[7] Z. Fan, L. Sun, Y. Huang, Y. Wang, M. Zhang, *Nat. Nanotechnol.* **2016**, *11*, 388.

[8] M. Khoshnejad, C. F. Greineder, K. W. Pulsipher, C. H. Villa, B. Altun, D. C. Pan, A. Tsourkas, I. J. Dmochowski, V. R. Muzykantov, *Bioconjug. Chem.* **2018**, *29*, 1209.

[9] X. Gao, S. Yang, C. Zhao, Y. Ren, D. Wei, *Angew. Chemie Int. Ed.* **2014**, *53*, 14027.

[10] P. Du, S. Xu, Z. Xu, Z. Wang, *Adv. Funct. Mater.* **2021**, *2104819*.

[11] M. Kanekiyo, C.-J. Wei, H. M. Yassine, P. M. McTamney, J. C. Boyington, J. R. R. Whittle, S. S. Rao, W.-P. Kong, L. Wang, G. J. Nabel, *Nature* **2013**, *499*, 102.

[12] J. H. Tian, N. Patel, R. Haupt, H. Zhou, S. Weston, H. Hammond, J. Logue, A. D. Portnoff, J. Norton, M. Guebre-Xabier, B. Zhou, K. Jacobson, S. Maciejewski, R.

Khatoon, M. Wisniewska, W. Moffitt, S. Kluepfel-Stahl, B. Ekechukwu, J. Papin, S. Boddapati, C. Jason Wong, P. A. Piedra, M. B. Frieman, M. J. Massare, L. Fries, K. L. Bengtsson, L. Stertman, L. Ellingsworth, G. Glenn, G. Smith, *Nat. Commun.* **2021**, *12*.

[13] S. C. Gilbert, S. L. Weinrich, R. Pruzan, L. Ma, M. Ouellette, V. M. Tesmer, S. E. Holt, A. G. Bodnar, S. Lichtsteiner, N. W. Kim, B. Trager, R. D. Taylor, R. Carlos, W. H. Andrews, W. E. Wright, J. Shay, C. B. Harley, G. B. Morin, *Nat. Biotechnol.* **1997**, *15*, 498.

[14] K. A. Collins, R. Snaith, M. G. Cottingham, S. C. Gilbert, A. V. S. Hill, *Sci. Rep.* **2017**, *7*, 46621.

[15] I. S. Georgiev, M. G. Joyce, R. E. Chen, K. Leung, K. McKee, A. Druz, J. G. Van Galen, M. Kanekiyo, Y. Tsybovsky, E. S. Yang, Y. Yang, P. Acharya, M. Pancera, P. V. Thomas, T. Wanninger, H. M. Yassine, U. Baxa, N. A. Doria-Rose, C. Cheng, B. S. Graham, J. R. Mascola, P. D. Kwong, *ACS Infect. Dis.* **2018**, *4*, 788.

[16] D. P. Patterson, A. M. Desai, M. M. B. Holl, E. N. G. Marsh, *RSC Adv.* **2011**, *1*, 1004.

[17] A. Ljubetič, F. Lapenta, H. Gradišar, I. Drobnak, J. Aupič, Ž. Strmšek, D. Lainšček, I. Hafner-Bratkovič, A. Majerle, N. Krivec, M. Benčina, T. Pisanski, T. Ć. Veličković, A. Round, J. M. Carazo, R. Melero, R. Jerala, *Nat. Biotechnol.* **2017**, *35*, 1094.

[18] J. A. J. Arpino, K. M. Polizzi, *ACS Synth. Biol.* **2020**, *9*, 993.

[19] G. A. Hudalla, T. Sun, J. Z. Gasiorowski, H. Han, Y. F. Tian, A. S. Chong, J. H. Collier, *Nat. Mater.* **2014**, *13*, 829.

[20] C. L. Hedegaard, C. Redondo-Gómez, B. Y. Tan, K. W. Ng, D. Loessner, A. Mata, *Sci. Adv.* **2020**, *6*, eabb3298.

[21] C. E. Mills, Z. Michaud, B. D. Olsen, *Biomacromolecules* **2018**, *19*, 2517.

[22] B. Israeli, D. S. Strugach, S. Gelkop, S. Weber, D. S. Gozlan, M. Amiram, *Adv. Funct. Mater.* **2021**, *2011276*.

[23] N. P. King, J. B. Bale, W. Sheffler, D. E. McNamara, S. Gonen, T. Gonen, T. O.

Yeates, D. Baker, *Nature* **2014**, *510*, 103.

[24] J. B. Bale, S. Gonen, Y. Liu, W. Sheffler, D. Ellis, C. Thomas, D. Cascio, T. O. Yeates, T. Gonen, N. P. King, D. Baker, *Science* **2016**, 353, 6297.

[25] R. Divine, H. V Dang, G. Ueda, J. A. Fallas, I. Vulovic, W. Sheffler, S. Saini, Y. T. Zhao, I. X. Raj, P. A. Morawski, M. F. Jennewein, L. J. Homad, Y.-H. Wan, M. R. Tooley, F. Seeger, A. Etemadi, M. L. Fahning, J. Lazarovits, A. Roederer, A. C. Walls, L. Stewart, M. Mazloomi, N. P. King, D. J. Campbell, A. T. McGuire, L. Stamatatos, H. Ruohola-Baker, J. Mathieu, D. Veesler, D. Baker, *Science* **2021**, *372*, eabd9994.

[26] S. Boyoglu-Barnum, D. Ellis, R. A. Gillespie, G. B. Hutchinson, Y.-J. Park, S. M. Moin, O. J. Acton, R. Ravichandran, M. Murphy, D. Pettie, N. Matheson, L. Carter, A. Creanga, M. J. Watson, S. Kephart, S. Ataca, J. R. Vaile, G. Ueda, M. C. Crank, L. Stewart, K. K. Lee, M. Guttman, D. Baker, J. R. Mascola, D. Veesler, B. S. Graham, N. P. King, M. Kanekiyo, *Nature* **2021**, *592*, 623.

[27] B. K. Shanbhag, B. Liu, J. Fu, V. S. Haritos, L. He, *Nano Lett.* **2016**, *16*, 3379.

[28] A. Aggeli, M. Bell, L. M. Carrick, C. W. G. Fishwick, R. Harding, P. J. Mawer, S. E. Radford, A. E. Strong, N. Boden, *J. Am. Chem. Soc.* **2003**, *125*, 9619.

[29] B. K. Shanbhag, C. Liu, V. S. Haritos, L. He, *ACS Nano* **2018**, *12*, 6956.

[30] M. Van Rosmalen, M. Krom, M. Merkx, *Biochemistry* **2017**, *56*, 6565.

[31] N. A. Díaz-Torres, B. P. Mahon, C. D. Boone, M. A. Pinard, C. Tu, R. Ng, M. Agbandje-McKenna, D. Silverman, K. Scott, R. McKenna, *Acta Crystallogr. Sect. D Biol. Crystallogr.* **2015**, *71*, 1745.

[32] M. Cortes-Clerget, N. Akporji, J. Zhou, F. Gao, P. Guo, M. Parmentier, F. Gallou, J. Y. Berthon, B. H. Lipshutz, *Nat. Commun.* **2019**, *10*, 2169.

[33] C. J. T. Robidillo, J. G. C. Veinot, *ACS Appl. Mater. Interfaces* **2020**, *12*, 52251.

[34] G. Young, N. Hundt, D. Cole, A. Fineberg, J. Andrecka, A. Tyler, A. Olerinyova, A. Ansari, E. G. Marklund, M. P. Collier, S. A. Chandler, O. Tkachenko, J. Allen, M.

Crispin, N. Billington, Y. Takagi, J. R. Sellers, C. Eichmann, P. Selenko, L. Frey, R. Riek, M. R. Galpin, W. B. Struwe, J. L. P. Benesch, P. Kukura, *Science* **2018**, *360*, 423.

[35] L. M. Carrick, A. Aggeli, N. Boden, J. Fisher, E. Ingham, T. a. Waigh, *Tetrahedron* **2007**, *63*, 7457.

[36] E. A. Berckman, W. Chen, *Chem. Commun.* **2019**, *55*, 8219.

[37] J. N. Vranish, M. G. Ancona, E. Oh, K. Susumu, G. Lasarte Aragonés, J. C. Breger, S. A. Walper, I. L. Medintz, *ACS Nano* **2018**, *12*, 7911.

[38] O. Pàmies, J. E. Bäckvall, *Chem. Rev.* **2003**, *103*, 3247.

[39] A. Liu, C. H. H. Traulsen, J. J. L. M. Cornelissen, *ACS Catal.* **2016**, *6*, 3084.

[40] Y. Si, Q. Tian, F. Zhao, S. H. Kelly, L. S. Shores, D. F. Camacho, A. I. Sperling, M. S. Andrade, J. H. Collier, A. S. Chong, *Sci. Adv*. **2020**, 6, eaba0995.

[41] J. Y. Oh, H. S. Kim, L. Palanikumar, E. M. Go, B. Jana, S. A. Park, H. Y. Kim, K. Kim, J. K. Seo, S. K. Kwak, C. Kim, S. Kang, J. H. Ryu, *Nat. Commun.* **2018**, *9*, 4548.

[42] Q. Fan, L. Li, H. Xue, H. Zhou, L. Zhao, J. Liu, J. Mao, S. Wu, S. Zhang, C. Wu, X. Li, X. Zhou, J. Wang, *Angew. Chemie - Int. Ed.* **2020**, *59*, 15141.

[43] E. P. Perillo, Y. L. Liu, K. Huynh, C. Liu, C. K. Chou, M. C. Hung, H. C. Yeh, A. K. Dunn, *Nat. Commun.* **2015**, *6*, 7874.

[44] J. Kim, W. Park, D. Kim, E. S. Lee, D. H. Lee, S. Jeong, J. M. Park, K. Na, *Adv. Funct. Mater.* **2019**, *29*, 1900084.

[45] M. S. Saveleva, K. Eftekhari, A. Abalymov, T. E. L. Douglas, D. Volodkin, B. V. Parakhonskiy, A. G. Skirtach, *Front. Chem.* **2019**, *7*, 179.

[46] A. Pourabed, T. Younas, C. Liu, B. K. Shanbhag, L. He, T. Alan, *J. Colloid Interface Sci.* **2020**, *585*, 229.

[47] J. Schindelin, I. Arganda-Carreras, E. Frise, V. Kaynig, M. Longair, T. Pietzsch, S. Preibisch, C. Rueden, S. Saalfeld, B. Schmid, J. Y. Tinevez, D. J. White, V.

Hartenstein, K. Eliceiri, P. Tomancak, A. Cardona, *Nat. Methods* **2012**, *9*, 676.

[48] J. I. Garzon, J. R. Lopéz-Blanco, C. Pons, J. Kovacs, R. Abagyan, J. Fernandez-Recio, P. Chacon, *Bioinformatics* **2009**, *25*, 2544.

[49] M. Sendovski, M. Kanteev, V. Shuster Ben-Yosef, N. Adir, A. Fishman, *Acta Crystallogr. Sect. F Struct. Biol. Cryst. Commun.* **2010**, *66*, 1101.

[50] M. Höhne, S. Schätzle, H. Jochens, K. Robins, U. T. Bornscheuer, *Nat. Chem. Biol.* **2010**, *6*, 807.

[51] M. D. Abràmoff, P. J. Magalhães, S. J. Ram, *Biophotonics Int.* **2004**, *11*, 36.

[52] N. M. Kirby, S. T. Mudie, A. M. Hawley, D. J. Cookson, H. D. T. Mertens, N. Cowieson, V. Samardzic-Boban, *J. Appl. Crystallogr.* **2013**, *46*, 1670.

[53] D. I. Svergun, *J. Appl. Crystallogr.* **1992**, *25*, 495.

Supporting Information

Custom design of protein particles as multifunctional biomaterials

Bhuvana K. Shanbhag, Chang Liu, Pradeep G.C., Tayyaba Younas, Kevin K.Y. Hu, Alex J. Fulcher, Weston B. Struwe, David Steer, Geoff Dumsday, Ian S. Harper, Philipp Kukura, Victoria S. Haritos, Lizhong He

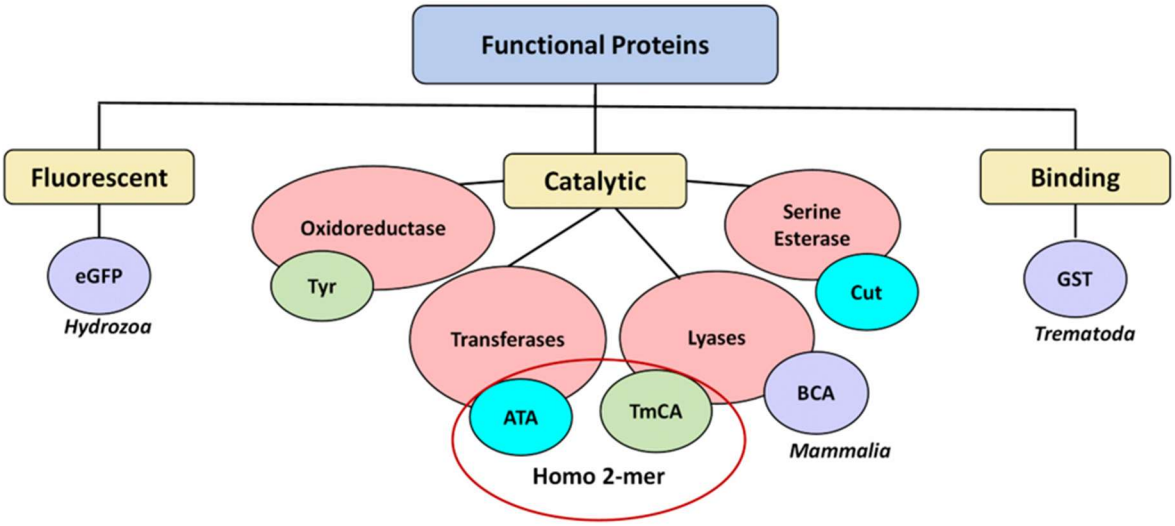

Figure S1. Assortment of functional proteins evaluated in this study for the formation of protein particles. Proteins with distinct functionalities, namely fluorescence, catalysis and binding, were obtained from different sources (green-bacteria, cyan-fungi, purple-animalia): eGFP-enhanced green fluorescent protein, Tyr-Tyrosinase, ATA-Aminotransaminase, TmCA-microbial carbonic anhydrase, BCA-Bovine carbonic anhydrase, Cut-Cutinase and GST- Glutathione-S-transferase. Proteins within red circle have dimeric conformation and other proteins have monomeric conformation.

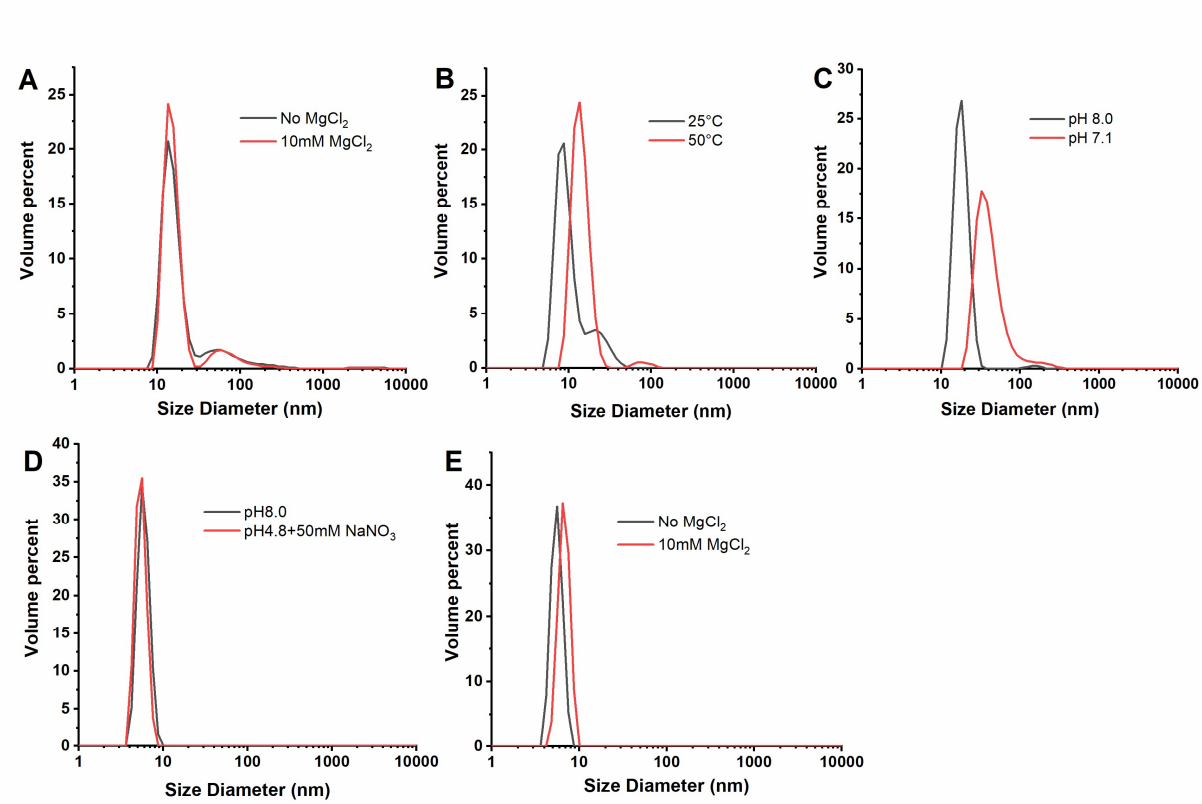

Figure S2. Particle size distributions for wild-type proteins under the assembly conditions used for formation of protein-peptide particles using dynamic light scattering. A) WT-Tyrosinase. B) WT-TmCA – thermostable carbonic anhydrase. C)WT-Aminotransaminase. D)WT-Cutinase. E) WT-eGFP. Black lines - absence of stimuli, Red lines- stimuli condition used for particle formation with the corresponding protein-peptide module.

Table S1. Functions and properties of protein candidates

	BCA	**TmCA**	**Tyr**	**Cut**	**ATA**	**GST**	**eGFP**
Full names	bovine carbonic anhydrase	thermostable carbonic anhydrase	tyrosinase	cutinase	ω-amino transferase	glutathione S-transferase	enhanced green fluorescent protein
Functions	Biocatalytic	Biocatalytic	Biocatalytic	Biocatalytic	Biocatalytic	Binding*	Fluorescent
Enzyme class	Lyases	Lyases	Oxidoreductase	Serine Esterase	Transferase	Transferase	N.A
Protein data bank ID	1V9E	4XZ5	4HD6	1AGY	4CE5	1UA5	4XOW
Source organism	Mammalia/Bos taurus	Bacteria/ *Thiomicrospira crunogena*	Bacteria/ *Bacillus megaterium*	Fungi / *Fusarium solani*	Fungi / *Aspergillus terreus*	Trematoda/ *Schistosoma japonicum*	Hydrozoa/ *Aequorea victoria*
Global Symmetry	Monomer	Homo 2-mer	Monomer	Monomer	Homo 2-mer	Homo 2-mer	Monomer
Active site Metal ion	Zn	Zn	Cu	None	None; co-factor dependant Pyridoxal-5'-phosphate (PLP)	N.A	N.A
Disulphide bonds	0	1	0	2	0	0	0
Reference	Ref [1]	Ref [2]	Ref [3]	Ref [4]	Ref [5]	Ref [6]	Ref [7]

* The strong binding ability of GST with its substrate, glutathione (GSH), makes it one of the most used binders in affinity chromatography.

Table S2. Peptide candidates and their properties

Peptide name	Amino acid Sequence	pI*	Charge at pH 7*	GRAVY	Reference
$P_{11}4$	$^{N-}$QQRFEWEFEQQ^{-C}	4.14	-2.1	-2.209	ref[8]
Q11	$^{N-}$QQKFQFQFEQQ^{-C}	6.25	-0.1	-1.818	ref[4]
Pep-H	$^{N-}$WFRFEWEFEFW^{-C}	4.14	-2.1	-0.591	This study

* calculated using Expasy Protparam tool, GRAVY: Grand average of hydropathicity

Table S3. Amino acid sequences of Protein-Peptide fusion constructs

Construct Name	Amino acid Sequence*
BCA-P$_{11}$4	GMSHHWGYGKHNGPEHWHKDFPIANGERQSPVDIDTKAVVQDP ALKPLALVYGEATSRRMVNNGHSFNVEYDDSQDKAVLKDGPLT GTYRLVQFHFHWGSSDDQGSEHTVDRKKYAAELHLVHWNTKYG DFGTAAQQPDGLAVVGVFLKVGDANPALQKVLDALDSIKTKGKS TDFPNFDPGSLLPNVLDYWTYPGSLTTPPLLESVTWIVLKEPISVSS QQMLKFRTLNFNAEGEPELLMLANWRPAQPLKNRQVRGFPKGG GGSGGGGSQQRFEWEFEQQ
BCA-Q11	GMSHHWGYGKHNGPEHWHKDFPIANGERQSPVDIDTKAVVQDP ALKPLALVYGEATSRRMVNNGHSFNVEYDDSQDKAVLKDGPLT GTYRLVQFHFHWGSSDDQGSEHTVDRKKYAAELHLVHWNTKYG DFGTAAQQPDGLAVVGVFLKVGDANPALQKVLDALDSIKTKGKS TDFPNFDPGSLLPNVLDYWTYPGSLTTPPLLESVTWIVLKEPISVSS QQMLKFRTLNFNAEGEPELLMLANWRPAQPLKNRQVRGFPKGG GGSGGGGSQQKFQFQFEQQ
BCA-Pep-H	GMSHHWGYGKHNGPEHWHKDFPIANGERQSPVDIDTKAVVQDP ALKPLALVYGEATSRRMVNNGHSFNVEYDDSQDKAVLKDGPLT GTYRLVQFHFHWGSSDDQGSEHTVDRKKYAAELHLVHWNTKYG DFGTAAQQPDGLAVVGVFLKVGDANPALQKVLDALDSIKTKGKS TDFPNFDPGSLLPNVLDYWTYPGSLTTPPLLESVTWIVLKEPISVSS QQMLKFRTLNFNAEGEPELLMLANWRPAQPLKNRQVRGFPKGG GGSGGGGSWFRFEWEFEFW
TmCA-P$_{11}$4	MGSSHHHHHHSSGLVPRGSHMANNVAAPLIDLGAEAKKQAQKS AATQSAVPEKESATKVAEKQKEPEEKAKPEPKKPPHWGYFGEEG PQYWGELAPEFSTCKTGKNQSPINLKPQTAVGTTSLPGFDVYYRE TALKLINNGHTLQVNIPLGSYIKINGHRYELLQYHFHTPSEHQRDG FNYPMEMHLVHKDGDGNLAVIAILFQEGEENETLAKLMSFLPQTL KKQEIHESVKIHPAKFFPADKKFYKYSGSLTTPPCSEGVYWMVFK QPIQASVTQLEKMHEYLGSNARPVQRQNARTLLKSWPDRNRANT VYEFYGGGGSGGGGSQQRFEWEFEQQ
Tyr-P$_{11}$4	MGSSHHHHHHSSGLVPRGSHMSNKYRVRKNVLHLTDTEKRDFV RTVLILKEKGIYDRYIAWHGAAGKFHTPPGSDRNAAHMSSAFLPW HREYLLRFERDLQSINPEVTLPYWEWETDAQMQDPSQSQIWSADF MGGNGNPIKDFIVDTGPFAAGRWTTIDEQGNPSGGLKRNFGATKE APTLPTRDDVLNALKITQYDTPPWDMTSQNSFRNQLEGFINGPQL HNRVHRWVGGQMGVGPTAPNDPVFFLHHANVDRIWAVWQIIHR NQNYQPMKNGPFGQNFRDPMYPWNTTPEDVMNHRKLGYVYDIE LRKSKRSSGGGGSGGGGSQQRFEWEFEQQ

Cut-P$_{11}$4	MGSSHHHHHHSSGLVPRGSHMLPTSNPAQELEARQLGRTTRDDLI NGNSASCADVIFIYARGSTETGNLGTLGPSIASNLESAFGKDGVWI QGVGGAYRATLGDNALPRGTSSAAIREMLGLFQQANTKCPDATLI AGGYSQGAALAAASIEDLDSAIRDKIAGTVLFGYTKNLQNRGRIP NYPADRTKVFCNTGDLVCTGSLIVAAPHLAYGPDARGPAPEFLIE KVRAVRGSAGGGGSGGGGSQQRFEWEFEQQ
ATA-P$_{11}$4	MGSSHHHHHHSSGLVPRGSHMASMDKVFAGYAARQAILESTETT NPFAKGIAWVEGELVPLAEARIPLLDQGFMHSDLTYDVPSVWDG RFFRLDDHITRLEASCTKLRLRLPLPRDQVKQILVEMVAKSGIRDA FVELIVTRGLKGVRGTRPEDIVNNLYMFVQPYVWVMEPDMQRVG GSAVVARTVRRVPPGAIDPTVKNLQWGDLVRGMFEAADRGATY PFLTDGDAHLTEGSGFNIVLVKDGVLYTPDRGVLQGVTRKSVINA AEAFGIEVRVEFVPVELAYRCDEIFMCTTAGGIMPITTLDGMPVNG GQIGPITKKIWDGYWAMHYDAAYSFEIDYNERNGGGGSGGGGSQ QRFEWEFEQQ
eGFP-P$_{11}$4	MGHHHHHHTDPMVSKGEELFTGVVPILVELDGDVNGHKFSVSGE GEGDATYGKLTLKFICTTGKLPVPWPTLVTTLAYGVLCFSRYPDH MKQHDFFKSAMPEGYVQERTIFFKDDGNYKTRAEVKFEGDTLVN RIELKGIDFKEDGNILGHKLEYNYNSHNVYIMADKQKNGIKSNFKI RHNIEDGSVQLADHYQQNTPIGDGPVLLPDNHYLSTQSKLSKDPN EKRDHMVLLEFVTAAGITLGMDELYKGGGGSGGGGSQQRFEWEF EQQ
eGFP-Pep-H	MGHHHHHHTDPMVSKGEELFTGVVPILVELDGDVNGHKFSVSGE GEGDATYGKLTLKFICTTGKLPVPWPTLVTTLAYGVLCFSRYPDH MKQHDFFKSAMPEGYVQERTIFFKDDGNYKTRAEVKFEGDTLVN RIELKGIDFKEDGNILGHKLEYNYNSHNVYIMADKQKNGIKSNFKI RHNIEDGSVQLADHYQQNTPIGDGPVLLPDNHYLSTQSKLSKDPN EKRDHMVLLEFVTAAGITLGMDELYKGGGGSGGGGSWFRFEWE FEFW
GST-P$_{11}$4	MGSSHHHHHHSSGLVPRGSHMSPILGYWKIKGLVQPTRLLLEYLE EKYEEHLYERDEGDKWRNKKFELGLEFPNLPYYIDGDVKLTQSM AIIRYIADKHNMLGGCPKERAEISMLEGAVLDIRYGVSRIAYSKDF ETLKVDFLSKLPEMLKMFEDRLCHKTYLNGDHVTHPDFMLYDAL DVVLYMDPMCLDAFPKLVCFKKRIEAIPQIDKYLKSSKYIAWPLQ GWQATFGGGDHPPKGGGGSGGGGSQQRFEWEFEQQ
GST-Q11	MGSSHHHHHHSSGLVPRGSHMSPILGYWKIKGLVQPTRLLLEYLE EKYEEHLYERDEGDKWRNKKFELGLEFPNLPYYIDGDVKLTQSM AIIRYIADKHNMLGGCPKERAEISMLEGAVLDIRYGVSRIAYSKDF ETLKVDFLSKLPEMLKMFEDRLCHKTYLNGDHVTHPDFMLYDAL DVVLYMDPMCLDAFPKLVCFKKRIEAIPQIDKYLKSSKYIAWPLQ GWQATFGGGDHPPKGGGGSGGGGSQQKFQFQFEQQ

* green - affinity tag for purification, purple - proteinase cleavage site, blue - GS linker, and red - self assembly peptide.

Table S4. Growth and protein expression conditions*

Condition	Protein Candidates						
	BCA	**TmCA**	**Tyr**	**Cut**	**ATA**	**eGFP**	**GST**
Initial growth	37°C 4hours	37°C 4hours	37°C 4hours	30°C 4hours	37°C 4hours	37°C 4hours	37°C 4hours
Induction method	Auto-Induction	IPTG	IPTG	IPTG	IPTG	Auto-Induction	IPTG
Inducer	0.2%v/v lactose	1mM	1mM	0.2mM	0.1mM	0.2%v/v lactose	1mM
Protein expression	20°C 16hours	20°C 16hours	20°C 16hours	20°C 16hours	25°C 16hours	20°C 16hours	20°C 16hours

* The growth and protein expression procedures were protein specific and the same procedures were used to express both wild type proteins and their respective protein-peptide constructs irrespective of the peptide type.

Table S5. Buffers used for protein-peptide purification*

Buffer	Protein candidates					
	BCA/eGFP	**TmCA**	**Tyr**	**Cut**	**ATA**	**GST**
Lysis buffer	50 mM Tris-HCl pH 8.0, 50 mM NaCl, 1 mM EDTA, 0.5% Triton-X 100	50 mM Tris-HCl pH 8.0, 50 mM NaCl, 1 mM EDTA, 0.5% Triton-X 100	50 mM Tris-HCl pH 8.0, 50 mM NaCl, and 0.5% Triton-X 100	BugBuster® Protein Extraction Reagent lysis buffer (Merck Millipore)	50mM Tris-HCl pH 7.5, 50 mM NaCl, 1 mM EDTA, 0.5% Triton-X 100 and 0.1mM co-factor Pyridoxal L phosphate-PLP	50 mM Tris-HCl pH 8.0, 50 mM NaCl, 1 mM EDTA, 0.5% Triton-X 100
IMAC buffer A	10 mM Tris-HCl buffer pH 8.0+0.5 M NaCl	50 mM Tris-HCl buffer pH 8.0+0.5 M NaCl	50 mM Tris-HCl buffer pH 7.5+0.5 M NaCl	20 mM Tris-HCl buffer pH 8.0+0.5 M NaCl	50 mM Tris-HCl buffer pH 7.5 containing 0.3 M NaCl	10 mM Tris-HCl buffer pH 8.0+0.5 M NaCl
IMAC buffer B	10 mM Tris-HCl buffer pH 8.0+0.5 M NaCl +0.2M imidazole	50 mM Tris-HCl buffer pH 8.0+0.5 M NaCl +0.2M imidazole	50 mM Tris-HCl buffer pH 7.5+0.5 M NaCl +0.2M imidazole	20 mM Tris-HCl buffer pH 8.0+0.5 M NaCl +1M imidazole	50 mM Tris-HCl buffer+0.3M NaCl pH 8.0+0.5M imidazole	10 mM Tris-HCl buffer pH 8.0+0.5 M NaCl +0.2M imidazole
Elution condition	Gradient elution 0 to 200mM imidazole	Step elution with 100,150, 200mM imidazole	Step elution with 50,100, 200mM imidazole	Step elution with 50,500, 1000mM imidazole	Step elution with 100, 200, 300, 500mM imidazole	Step elution with 50,100, 200mM imidazole
Desalting buffer	10 mM Tris-HCl, pH 8	50 mM Tris-HCl buffer pH 8.0+0.2 M NaCl	10 mM Tris-HCl buffer pH 7.5	20 mM Tris-HCl buffer pH 6.5	20 mM Tris-HCl buffer pH 7.5+0.01mM co-factor Pyridoxal L phosphate-PLP	10 mM Tris-HCl, pH 8

* The purification procedures used were protein specific and the same procedures were used to purify wild type proteins and their respective protein-peptide constructs irrespective of the peptide type.

Table S6. Optimal conditions for protein particle formation*

Protein-peptide system	Particle forming conditions				
	Protein Buffer	**Stimuli type**	**Stimulus agent**	**Incubation time**	**Final Solution condition**
BCA-P114	50mM Tris-HCl pH8.0	pH	5 M or 1 M acetic acid	5 mins	pH 6.8
	10mM Tris-HCl pH8.0	metal ion	0.5 M $MgCl_2$ in 10 mM Tris-HCl pH8.0	5 mins	5-20 mM
BCA-Q11	50mM Tris-HCl pH8.0	pH	5 M or 1 M acetic acid	5 mins	pH 7.0
BCA-Pep-H	50mM Tris-HCl pH8.0	pH	5 M or 1 M acetic acid	5 mins	pH 6.8
	10mM Tris-HCl pH8.0	metal ion	0.5 M $MgCl_2$ in 10 mM Tris-HCl pH8.0	5 mins	5-20 mM
TmCA-P114	50mM Tris-HCl pH8.0+0.2M NaCl	Temperature	Heat	1 min	50°C
Tyr-P114	10mM Tris-HCl pH7.5	metal ion	0.5 M $MgCl_2$ in 10 mM Tris-HCl pH7.5	2-5 mins	10 mM
Cut-P114	20mM Tris-HCl pH6.5	pH + ionic strength	5 M or 1 M acetic acid and 0.5 M $NaNO_3$ in 10 mM Tris-HCl pH 6.5	2-5 mins	pH 4.8 + 50 mM $NaNO_3$
ATA-P114	50mM Tris-HCl pH8.0	pH	5 M or 1 M acetic acid	5 mins	pH 7.1
eGFP-P114	10mM Tris-HCl pH8.0	metal ion	0.5 M $MgCl_2$ in 10 mM Tris-HCl pH 8.0	5 mins	10 mM
eGFP-Pep-H	10mM Tris-HCl pH8.0	metal ion	0.5 M $MgCl_2$ in 10 mM Tris-HCl pH 8.0	5 mins	5-20 mM
GST-P114	50mM Tris-HCl pH8.0	pH	5 M or 1 M acetic acid	5 mins	pH 6.0
	10mM Tris-HCl pH8.0	metal ion	0.5 M $MgCl_2$ in 10 mM Tris-HCl pH 8.0	5 mins	5-20 mM
GST-Q11	50mM Tris-HCl pH8.0	pH	5 M or 1 M acetic acid	5 mins	pH 6.7

* Typical protein concentration used was in the range of 0.2-0.5 mg/mL.

Table S7. Conditions for protein particle formation demonstrated in Fig. 2*

Sub-figure number	Protein-peptide system	Tested condition		
		Protein buffer	Stimulus agent	Final Solution condition
2b	BCA-Pep-H eGFP-Pep-H	10 mM Tris-HCl pH 8.0	No stimulus	10 mM Tris-HCl pH 8.0
2c	BCA-Pep-H eGFP-Pep-H	10 mM Tris-HCl pH8.0	0.5 M $MgCl_2$ in 10 mM Tris-HCl pH 8.0	10 mM Tris-HCl pH 8.0 +10 mM $MgCl_2$
2d	BCA-Pep-H	50 mM Tris-HCl pH 8.0	5 M or 1M acetic acid	pH 6.8
2g	BCA-Q11 GST-Q11	10 mM Tris-HCl pH 8.0	0.5 M $MgCl_2$ in 10 mM Tris-HCl pH 8.0	10 mM Tris-HCl pH 8.0 +20 mM $MgCl_2$
2h	BCA-Q11	50 mM Tris-HCl pH 8.0	5 M or 1 M acetic acid	pH 7.0
	GST-Q11			pH 6.7
2i	BCA-$P_{11}4$ eGFP-$P_{11}4$	10 mM Tris-HCl pH 8.0	0.5 M $MgCl_2$ in 10 mM Tris-HCl pH 8.0	10 mM Tris-HCl pH 8.0 +10 mM $MgCl_2$
	GST-$P_{11}4$			10 mM Tris-HCl pH 8.0 +20 mM $MgCl_2$
2j	BCA-$P_{11}4$	50 mM Tris-HCl pH 8.0	5 M or 1 M acetic acid	pH 7.0
	eGFP-$P_{11}4$			pH 6.7

* Protein concentration used was 0.5 mg/mL

References

[1] R. Saito, T. Sato, A. Ikai, N. Tanaka, *Acta Crystallogr. Sect. D Biol. Crystallogr.* **2004**, *60*, 792.

[2] N. A. Díaz-Torres, B. P. Mahon, C. D. Boone, M. A. Pinard, C. Tu, R. Ng, M. Agbandje-McKenna, D. Silverman, K. Scott, R. McKenna, *Acta Crystallogr. Sect. D Biol. Crystallogr.* **2015**, *71*, 1745.

[3] M. Sendovski, M. Kanteev, V. Shuster Ben-Yosef, N. Adir, A. Fishman, *Acta Crystallogr. Sect. F Struct. Biol. Cryst. Commun.* **2010**, *66*, 1101.

[4] G. A. Hudalla, T. Sun, J. Z. Gasiorowski, H. Han, Y. F. Tian, A. S. Chong, J. H. Collier, *Nat. Mater.* **2014**, *13*, 829.

[5] M. Höhne, S. Schätzle, H. Jochens, K. Robins, U. T. Bornscheuer, *Nat. Chem. Biol.* **2010**, *6*, 807.

[6] I. Kursula, A. M. Heape, P. Kursula, *Protein Pept. Lett.* **2005**, *12*, 709.

[7] S. Duwé, E. De Zitter, V. Gielen, B. Moeyaert, W. Vandenberg, T. Grotjohann, K. Clays, S. Jakobs, L. Van Meervelt, P. Dedecker, *ACS Nano* **2015**, *9*, 9528.

[8] S. E. R. A. Aggeli, M.Bell, N.Boden, J.N. Keen, P.F.Knowles, T.C.B.McLeish, M.Pitkeathly, *Nature* **1997**, *386*, 259.